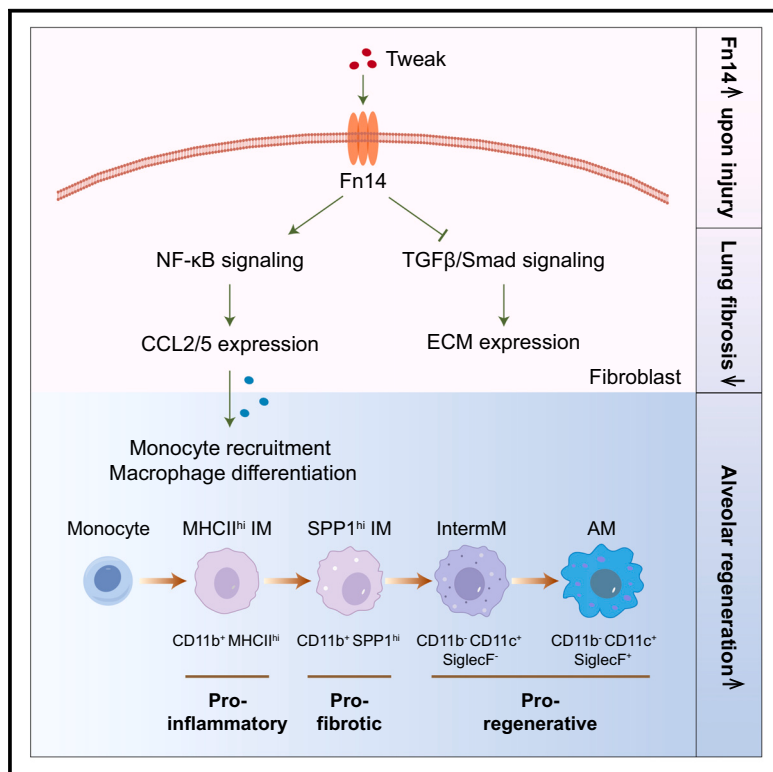


# TWEAK-Fn14 signaling protects mice from pulmonary fibrosis by inhibiting fibroblast activation and recruiting pro-regenerative macrophages

## Graphical abstract



## Authors

Li Liu, Pei Wu, Yuqi Wei, ..., Xiaoyong Shen, Lingyun Sun, Ying Xi

## Correspondence

xiucheng\_liu@outlook.com (X.L.),  
xiaoyongshen@fudan.edu.cn (X.S.),  
lingyunsun@nju.edu.cn (L.S.),  
xiying@shanghaitech.edu.cn (Y.X.)

## In brief

Liu et al. demonstrated a protective role of TWEAK-Fn14 signaling in lung fibrosis. Fn14 deficiency promotes fibroblast activation thus increasing ECM production, impairs macrophage infiltration in the lung and diminishes pro-regenerative IntermM and AM subpopulations, leading to impaired alveolar regeneration and exacerbated lung fibrosis.

## Highlights

- TWEAK-Fn14 signaling inhibits TGFβ signaling and ECM synthesis in fibroblasts
- TWEAK-Fn14 signaling induces chemokine expression to recruit macrophages
- Fn14 deficiency diminishes intermediate macrophages, which promote alveolar regeneration
- TWEAK-Fn14 signaling plays a protective role in pulmonary fibrosis



## Article

# TWEAK-Fn14 signaling protects mice from pulmonary fibrosis by inhibiting fibroblast activation and recruiting pro-regenerative macrophages

Li Liu,<sup>1,2,7</sup> Pei Wu,<sup>1,2,7</sup> Yuqi Wei,<sup>1</sup> Meng Lu,<sup>1,2</sup> Haiyan Ge,<sup>3</sup> Ping Wang,<sup>1,2</sup> Jianlong Sun,<sup>1,2</sup> Tiffany Horng,<sup>1</sup> Xiucheng Liu,<sup>4,\*</sup> Xiaoyong Shen,<sup>5,\*</sup> Lingyun Sun,<sup>6,\*</sup> and Ying Xi<sup>1,2,8,\*</sup>

<sup>1</sup>School of Life Science and Technology, ShanghaiTech University, Shanghai 201210, China

<sup>2</sup>State Key Laboratory of Advanced Medical Materials and Devices, ShanghaiTech University, Shanghai 201210, China

<sup>3</sup>Department of Pulmonary and Critical Care Medicine, Huadong Hospital Affiliated to Fudan University, Shanghai 200040, China

<sup>4</sup>Department of Thoracic Surgery, Shanghai Pulmonary Hospital, Tongji University School of Medicine, Shanghai 200433, China

<sup>5</sup>Department of Thoracic Surgery, Huadong Hospital Affiliated to Fudan University, Shanghai 200040, China

<sup>6</sup>Department of Rheumatology and Immunology, Nanjing Drum Tower Hospital, Affiliated Hospital of Medical School, Nanjing University, Nanjing 210008, China

<sup>7</sup>These authors contributed equally

<sup>8</sup>Lead contact

\*Correspondence: xiucheng\_liu@outlook.com (X.L.), xiaoyongshen@fudan.edu.cn (X.S.), lingyunsun@nju.edu.cn (L.S.), xiying@shanghaitech.edu.cn (Y.X.)

<https://doi.org/10.1016/j.celrep.2024.115220>

## SUMMARY

Idiopathic pulmonary fibrosis (IPF) is a fatal lung disease characterized by excess accumulation of the extracellular matrix (ECM). The role of macrophage-fibroblast crosstalk in lung fibrogenesis is incompletely understood. Here we found that fibroblast growth factor-inducible molecule 14 (Fn14), the receptor for tumor necrosis factor-like weak inducer of apoptosis (TWEAK) is highly induced in myofibroblasts in the lungs of IPF patients and the bleomycin-induced lung fibrosis model. TWEAK-Fn14 signaling inhibits fibroblast activation and ECM synthesis and induces chemokine expression to recruit monocytes/macrophages into the lung. Fn14 deficiency increases ECM production and impairs macrophage infiltration and differentiation, leading to exacerbated lung fibrosis and impaired alveolar regeneration in a bleomycin model. Interestingly, Fn14 deficiency diminishes an injury-induced SiglecF<sup>-</sup> CD11b<sup>-</sup> MHCII<sup>lo</sup> intermediate macrophage (InterMM) subpopulation, which promotes alveolar type II (AT2) cell proliferation in organoid cultures. These results collectively demonstrate a protective role of TWEAK-Fn14 signaling in lung fibrosis, highlighting the complexities and multilayered regulation of macrophage-fibroblast crosstalk.

## INTRODUCTION

Idiopathic pulmonary fibrosis (IPF) is a chronic and progressive lung disease with a median survival time of 2–3 years.<sup>1,2</sup> So far, two medications, nintedanib and pirfenidone, have been approved for the treatment of IPF, but they can only slow down the progression of lung fibrosis and cannot reverse fibrosis. Lung transplantation remains the only cure. Thus, in-depth understanding of IPF pathogenesis is essential for developing new therapeutic strategy. It is generally accepted that IPF arises from an aberrant wound healing process induced by repetitive alveolar epithelial injuries. Immune cells and fibroblasts are recruited to the sites of injuries, where fibroblasts are activated and deposit excessive extracellular matrix (ECM) components, leading to fibrosis and lung function decline.<sup>3–5</sup>

Macrophages are the most abundant immune cells that reside in the lung at homeostasis and play an essential role in fibrogenesis.<sup>6</sup> Macrophages engage in crosstalk with fibroblasts, and such crosstalk has been implicated in fibrosis.<sup>6–8</sup> In the steady

state and during fibrosis, fibroblasts provide colony-stimulating factor 1 (CSF1) to maintain macrophage survival, proliferation, and differentiation.<sup>7–9</sup> In the fibrotic lungs, activated fibroblasts secret chemokines such as C-C motif chemokine ligand 2 (CCL2), to recruit macrophages to fibrotic lesions.<sup>7</sup> On the other hand, macrophages release proinflammatory cytokines, such as tumor necrosis factor  $\alpha$  (TNF $\alpha$ ), interleukin 1 (IL-1), and interleukin 6 (IL-6), as well as profibrotic factors, such as transforming growth factor  $\beta$  (TGF $\beta$ ), which is a master regulator of fibroblast activation and tissue fibrosis.<sup>3,10–12</sup> They also secret growth factors like platelet-derived growth factor (PDGF), fibroblast growth factor (FGF), and amphiregulin (AREG) to promote fibroblast proliferation, and matrix metalloproteinases (MMPs) to remodel the ECM.<sup>5,7,13,14</sup>

Besides proinflammatory and profibrotic effects, monocytes and M2-like macrophages, recruited through the CCL2-CCR2 axis, have been shown to promote AT2 proliferation and alveolar regeneration during pneumonectomy-induced lung regeneration.<sup>15</sup> AT2s are the alveolar stem cells and can self-renew and



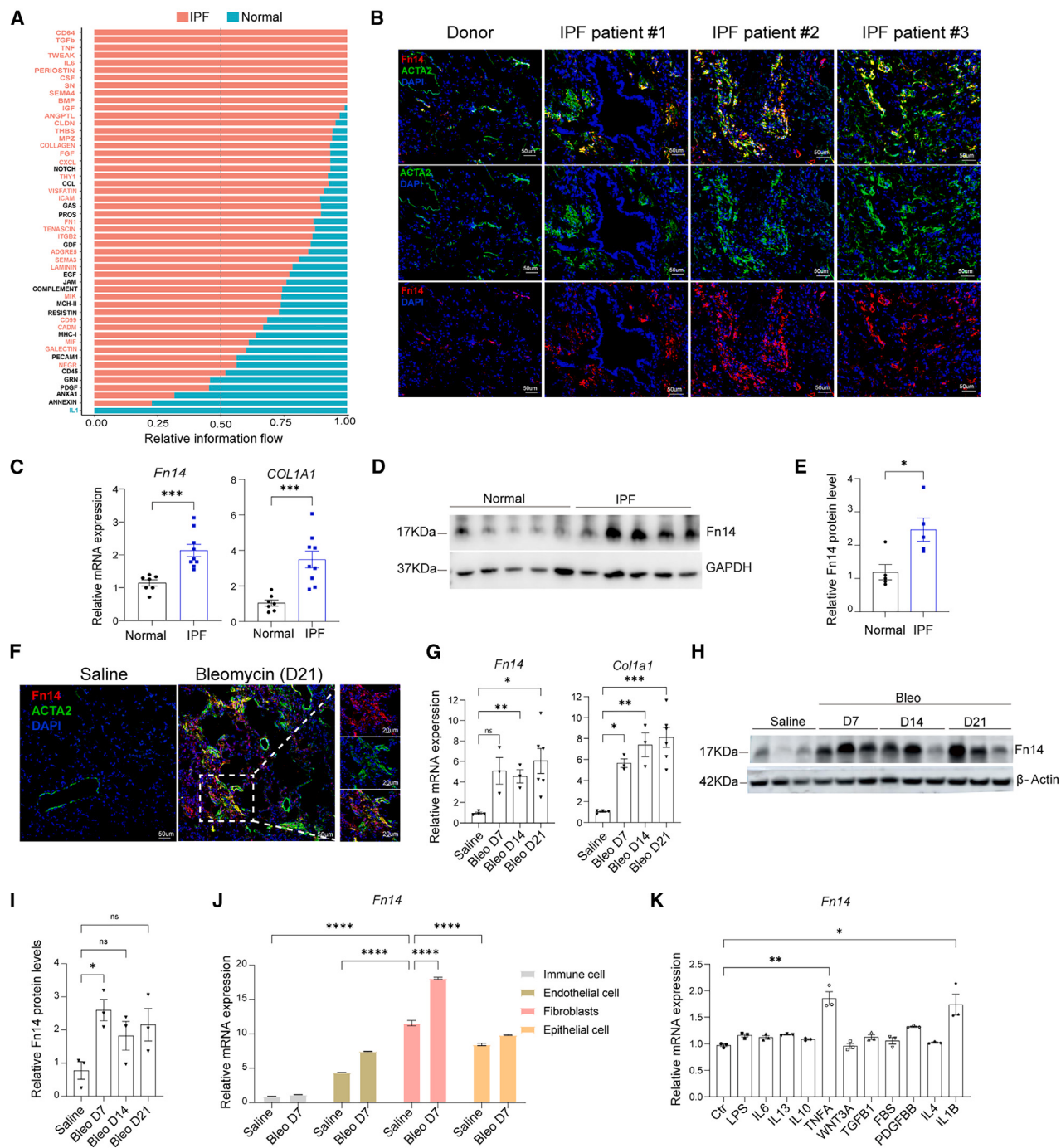


**Figure 1. scRNA-seq analysis reveals TWEAK-Fn14 signaling is upregulated in fibrotic lungs**

(A) CellChat analysis of publicly available scRNA-seq data (GEO: GSE135893)<sup>34</sup> predicting signaling pathways mediating macrophage and fibroblast crosstalk. The signaling pathways in red are enriched in IPF; the black ones are equally enriched in IPF and normal; the green ones are enriched in normal.

(B) Representative images of Fn14 immunofluorescence in human lungs. The myofibroblast marker ACTA2 (green), Fn14 (red), DAPI (blue). Scale bar, 50 $\mu$ m.

(C) Relative mRNA levels of Fn14 and COL1A1 in normal and IPF lungs. Normal, n = 7 donors; IPF, n = 9 donors.

(D and E) Representative immunoblots (D) and quantification (E) of Fn14 expression in normal and IPF lungs. GAPDH is a loading control for whole-lung lysates.

(F) Representative images of Fn14 immunofluorescence in mouse lungs. ACTA2 (green), Fn14 (red), DAPI (blue). Scale bar, 50 $\mu$ m, 20  $\mu$ m.

(G) Relative Fn14 and Col1a1 mRNA levels in mouse lungs treated with bleomycin. Saline, n = 4 mice; Bleo D7, n = 3 mice; Bleo D14, n = 3 mice; Bleo D21, n = 6 mice.

(legend continued on next page)

give rise to alveolar type I cells (AT1s) during homeostasis and after injury.<sup>16</sup> Interstitial macrophage (IM)-derived IL-1 $\beta$  has been shown to promote AT2 proliferation and differentiation into AT1s, but chronic inflammation mediated by IL-1 $\beta$  prevents AT1 differentiation, leading to impaired alveolar regeneration and fibrogenesis.<sup>17</sup> Therefore, the role of macrophages in fibrosis is complicated. Recently, with the advent of single-cell technologies, macrophage heterogeneity has been assessed in a completely unbiased manner. Several profibrotic subpopulations have been identified, including CX3CR1 $^+$  SiglecF $^+$  macrophages in mouse lungs<sup>18</sup> and SPP1 $^{hi}$  macrophages<sup>19,20</sup> and CD163 $^+$  macrophages<sup>21,22</sup> in human lungs. The absence of Lyve1 $^{hi}$  MHCII $^{lo}$  CX3CR1 $^{lo}$  monocyte-derived IMs exacerbated bleomycin-induced lung fibrosis,<sup>23</sup> suggesting an antifibrotic role of macrophage subpopulation. Better characterization of the heterogeneity and function of macrophage subpopulations is needed to understand the pathogenesis of pulmonary fibrosis.

Tumor necrosis factor-like weak inducer of apoptosis (TWEAK), also known as TNFSF12, is a multifunctional cytokine that controls many cellular activities in tissue repair and disease by binding to its receptor fibroblast growth factor-inducible molecule 14 (Fn14).<sup>24,25</sup> TWEAK-Fn14 signaling has been shown to induce canonical and noncanonical nuclear factor (NF- $\kappa$ B signaling, triggering proinflammatory responses and leukocyte infiltration.<sup>24–26</sup> It is reported to promote liver and kidney fibrosis by inducing fibroblast proliferation, migration, or activation<sup>27,28</sup> and is involved in tumor growth and invasion.<sup>29</sup> It also can promote the proliferation of liver progenitor cells<sup>30</sup> and skeletal muscle precursor cells,<sup>31</sup> involved in tissue repair and regeneration as well as mammalian epithelial branching morphogenesis.<sup>32</sup> So far, the role of this signaling axis in lung fibrosis is not reported.

Here, we demonstrated that TWEAK-Fn14 signaling functions as a protective mechanism against lung fibrosis. TWEAK-Fn14 signaling, upregulated in the (myo)fibroblasts of fibrotic lungs, inhibits the TGF $\beta$  signaling pathway and ECM production. TWEAK-Fn14 signaling also induces chemokine expression to recruit monocytes into the lung and promote macrophage differentiation. Fn14-knockout (KO) mice exhibit exacerbated lung fibrosis post bleomycin injury, with increased ECM production in the (myo)fibroblasts, decreased macrophage infiltration and differentiation, and impaired alveolar epithelial cell proliferation. This study provides new insights into macrophage-fibroblast crosstalk in fibrotic lungs.

## RESULTS

### TWEAK-Fn14 signaling is upregulated in fibrotic lungs

To explore macrophage-fibroblast interactions occurring in lung fibrosis, we used the CellChat algorithm<sup>33</sup> to analyze publicly

available small-cell RNA sequencing (scRNA-seq) data from IPF and normal human lungs (GEO: GSE135893) focusing on macrophages and fibroblasts.<sup>34</sup> Information flow analysis identified 33 signaling pathways that were enriched in either IPF or normal lungs (Figure 1A), with TGF $\beta$  and TNF $\alpha$  signaling among the top-ranked upregulated pathways in IPF lungs. Notably, TWEAK-Fn14 signaling was also highly upregulated in IPF lungs; this pathway has been reported to regulate interactions between immune cells and various cell types such as stromal, epithelial, and endothelial cells in tissue injury, inflammatory diseases, and cancers.<sup>26,35</sup>

Fn14 levels are typically low in healthy tissues, with TWEAK-Fn14 signaling activated in tissue injury and disease by increased Fn14 expression.<sup>24,35</sup> The scRNA-seq data<sup>33</sup> showed that Fn14 mRNA level was low in normal lungs and highly induced in IPF lung fibroblasts, while TWEAK was mainly expressed in macrophages in normal lungs and reduced in IPF lung macrophages (Figure S1A). To validate the scRNA-seq results, we examined Fn14 expression in the lungs from nine end-stage IPF patients undergoing lung transplantation and seven healthy donors. Immunofluorescence staining showed Fn14 was undetectable in healthy lungs; in IPF lungs, there was a strong Fn14 signal in ACTA2-expressing myofibroblasts (Figure 1B). qPCR and immunoblotting of lung lysates confirmed that Fn14 expression was significantly upregulated in IPF lungs compared with healthy controls (Figures 1C–1E), while TWEAK expression was decreased in IPF lungs (Figure S1B–S1C).

We observed a similar expression pattern in the widely used bleomycin-induced murine lung fibrosis model. A single intratracheal instillation of bleomycin induces acute lung injury and inflammation that peaks around day 7, followed by a profibrotic phase around day 14 to day 21.<sup>36</sup> The Fn14 protein was undetectable in saline control lungs, but was evident in the bleomycin-injured lungs at 21 days, with an obvious induction in ACTA2-expressing myofibroblasts (Figure 1F). qPCR and immunoblotting showed elevated Fn14 levels in the injured lungs at all examined time points (Figure 1G–1I), while TWEAK mRNA and protein levels were decreased after bleomycin injury (Figure S1D and S1E).

We further analyzed Fn14 and TWEAK expression in a published scRNA-seq database of bleomycin-injured mouse lungs.<sup>37</sup> Fn14 expression was upregulated in both fibroblasts and alveolar epithelial cells, and *Tweak* was highly expressed by fibroblasts in steady state and downregulated after bleomycin injury, while immune-cell-expressing *Tweak* was increased after injury (Figure S1F). In order to confirm the scRNA-seq results, we flow sorted different cell populations from saline- and bleomycin-treated lungs and examined Fn14 and *Tweak* expression by qPCR. Fibroblasts had the highest expression of Fn14 and *Tweak* among all the cell types. Fn14 expression in fibroblasts

(H and I) Representative immunoblots (H) and quantification (I) of Fn14 expression at indicated time points post bleomycin injury.  $\beta$ -Actin is a loading control for whole-lung lysates.

(J) Fn14 expression in different populations of the saline- and bleomycin-injured lungs at day 7.  $n = 3$  biological replicates representing nine mice/group.

(K) Relative mRNA levels of Fn14 in mouse lung fibroblasts after treatment with multiple cytokine and growth factors.  $n = 3$  biological replicates. Data in (C), (E), (G), and (I)–(K) represent mean  $\pm$  standard error of the mean (SEM). Similar results were observed in at least three independent experiments.  $p$  value is calculated using (C) and (E), two-tailed t test; (G), (I), and (K), one-way ANOVA; and (J), two-way ANOVA. \*\*\* $p < 0.001$ , \*\* $p < 0.01$ , \* $p < 0.05$ . NS, not significant. See also Figure S1.

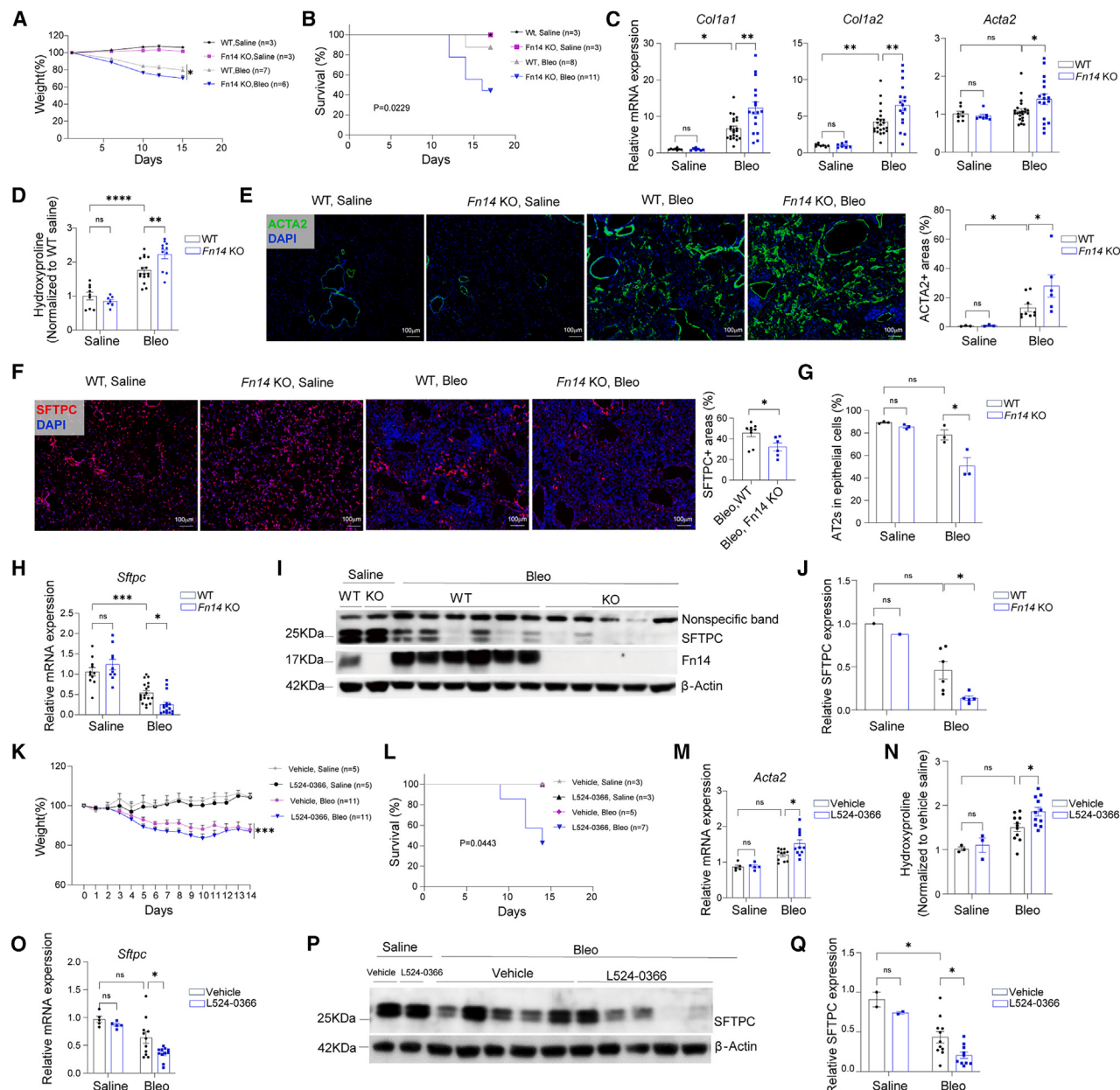


**Figure 2. Fn14 deficiency exacerbates bleomycin-induced lung fibrosis**

(A and B) The body weight (A) and survival rate (B) of bleomycin-injured WT and Fn14-KO mice by day 17.

(C) Fibrotic gene *Col1a1*, *Col1a2*, and *Acta2* expression in the WT and Fn14-KO lungs on day 14. Saline/WT, n = 8 mice; saline/KO, n = 7 mice; bleo/WT, n = 22 mice; bleo/KO, n = 17 mice.

(D) Hydroxyproline content of the WT and Fn14-KO lungs on day 14. Saline/WT, n = 9 mice; saline/KO, n = 7 mice; bleo/WT, n = 16 mice; bleo/KO, n = 11 mice.

(E) Representative images (left) and quantification (right) of ACTA2 immunofluorescence staining in the WT and Fn14-KO lungs on day 14. Saline/WT, n = 3 mice; saline/KO, n = 3 mice; bleo/WT, n = 9 mice; bleo/KO, n = 6 mice. Scale bar, 100 μm.

(F) Representative images (left) and quantification (right) of SFTPC immunofluorescence staining in the WT and Fn14-KO lungs on day 14. Bleo/WT, n = 9 mice; bleo/KO, n = 6 mice. Scale bar, 100 μm.

(G) Quantification of AT2 percentage in epithelial cells in the WT and Fn14-KO lungs on day 14. n = 3 mice/group.

(H) *Sftpc* mRNA levels in the WT and Fn14-KO lungs on day 14. Saline/WT, n = 11 mice; saline/KO, n = 7 mice; bleo/WT, n = 22 mice; bleo/KO, n = 17 mice.

(I and J) Representative immunoblots (I) and quantification (J) of WT and Fn14-KO mouse lung lysates on day 14. β-Actin is a loading control for whole-lung lysates.

(K-O) The body weight (K), survival rate (L), *Acta2* expression (M), hydroxyproline content (N), and *Sftpc* mRNA levels (O) of L524-0366 and vehicle control-treated mice on day 14. Saline, n = 5 mice/group; bleo, n = 11 mice/group.

(legend continued on next page)

was further induced by bleomycin injury, while epithelial *Fn14* expression was not upregulated (Figure 1J). *Tweak* expression in fibroblasts was significantly reduced after injury, while *Tweak* in immune cells was upregulated (Figure S1G).

*Fn14* expression was previously found to be injury-induced, with demonstrated regulation by multiple growth factors and cytokines.<sup>24</sup> Through a screen of a variety of profibrotic and proinflammatory growth factors and cytokines using primary mouse lung fibroblast cultures, we found that TNF $\alpha$  and IL-1 $\beta$ —proinflammatory factors previously shown to be induced by bleomycin injury<sup>3</sup>—each induced *Fn14* expression (Figure 1K). Together, the results from clinical samples and a murine injury model collectively support elevated *Fn14* levels in the (myo)fibroblasts of fibrotic lungs, suggesting a role of *Fn14* in fibrogenesis.

#### ***Fn14* deficiency exacerbates bleomycin-induced lung fibrosis in mouse model**

We subsequently explored the specific impact of *Fn14* in lung fibrosis by generating *Fn14* KO mice using CRISPR-Cas9. Sequencing of genomic DNA confirmed the desired deletion of five base pairs resulting in a frameshift after the 24th amino acid, which is in the extracellular domain and thus early termination of translation at the 36th amino acid (Figure S2A). Immunoblotting of lysates from the lung, stomach, and liver confirmed successful *Fn14* knockout (Figure S2B). The mice developed and bred normally without obvious defects.

Upon bleomycin injury, the *Fn14*-KO mice displayed more severe body weight loss compared with wild-type (WT) controls (Figure 2A) and had a significantly reduced survival rate (Figure 2B); indeed, the deleterious outcomes were so severe that we were unable to wait until the prespecified day 21 to euthanize the mice. On day 14, when the fibrotic phase of the injury model begins, the *Fn14*-KO mice had more severe lung fibrosis than WT controls, as assessed by qPCR measuring fibrillar collagen expression (*Col1a1* and *Col1a2*) and the myofibroblast marker *Acta2* (Figure 2C) as well as hydroxyproline assay measuring collagen content (Figure 2D). We also observed a significant increase in the area of ACTA2-expressing myofibroblasts in the *Fn14*-KO mice (Figure 2E), suggesting there were more myofibroblasts in the KO group.

Previous studies have established that bleomycin initially damages the alveolar epithelium, which induces immune cell infiltration and fibroblast migration, activation, and proliferation, ultimately leading to lung fibrosis. Impaired alveolar repair has been linked to lung fibrogenesis.<sup>37–41</sup> Bleomycin injury damages both AT1 and AT2 cells. *Fn14* deficiency further reduced AT2 cell number and SFTPC expression after bleomycin injury but had no obvious effects at steady state (Figures 2F–2J). AT1 marker *Rage* was also decreased in the *Fn14*-KO mice (Figure S3A).

To examine whether lung injury was affected by *Fn14* KO, we examined an early time point day 7 when inflammation peaks. There was no difference in the protein levels in bronchoalveolar

lavage fluid (BALF), AT2 and AT1 marker expression, and lung histology (Figure S3B–S3F), suggesting similar extent of lung injury. To explore the possibility that the higher mortality observed in *Fn14*-KO mice was due to other organ defects, we collected livers, kidneys, small intestines, hearts, and pancreas for histology examination. No significant abnormalities were observed (Figure S4). In conclusion, *Fn14* deficiency impedes alveolar repair and exacerbates lung fibrosis in the bleomycin model.

To validate our results obtained from *Fn14*-KO mice, we used *Fn14* antagonist L524-0366, which is a triazolyl-thiomorpholinyl-methanone compound that competes against TWEAK for *Fn14* binding.<sup>42,43</sup> Compared with the vehicle control, the mice injected with L524-0366 had more weight loss, higher mortality, and increased collagen content and myofibroblast marker expression (Figures 2K–2N), indicating more severe lung fibrosis, consistent with the phenotype observed in *Fn14* KO. Moreover, alveolar repair was also impaired in the antagonist treated group (Figures 2O–2Q and S3G). Taken together, both *Fn14* deficiency and antagonism impair alveolar repair and exacerbate lung fibrosis in bleomycin model.

#### **TWEAK inhibits fibroblast activation and ECM synthesis and induces chemokine expression in both lung fibroblast cultures and *in vivo***

To understand how *Fn14* deficiency induces exacerbation of lung fibrosis, we examined the role of TWEAK-*Fn14* signaling in mouse lung fibroblasts (MLFs). Recombinant TWEAK protein had no obvious effects on the proliferation or migration of primary MLFs (Figure S5A–S5D). We therefore conducted an exploratory RNA-seq analysis of TWEAK-stimulated primary MLFs to assess the potential role. Primary MLFs were stimulated with TWEAK for 48 h. RNA-seq analysis followed by Gene Ontology (GO) analysis of the differential expressed genes (DEGs) revealed that “collagen-containing extracellular matrix” is the top GO enriched in the downregulated genes ( $\text{Log}_2\text{FC} \leq -1$ ,  $p$  value  $\leq 0.05$ ) (Figure 3A, Table S1). The expression of ECM genes, including *Col1a1*, *Col1a2*, *Col3a1*, and *Fn1*, as well as myofibroblast marker *Acta2*, were all significantly reduced by TWEAK stimulation in a dose-dependent manner (Figure 3B), suggesting TWEAK inhibits ECM synthesis.

TGF $\beta$ 1 is a master regulator of ECM accumulation.<sup>3,12</sup> Upon TGF $\beta$ 1 stimulation, fibroblasts are activated and transdifferentiate into myofibroblasts, which have increased ECM synthesis and expression of contractile proteins, such as  $\alpha$ -smooth muscle actin (encoded by *Acta2*). We then examined the effects of TWEAK in the presence of TGF $\beta$ 1. TWEAK inhibited both baseline and TGF $\beta$ 1 induced fibroblast activation and ECM production in MLFs (Figures 3C and 3D). TGF $\beta$ 1 signals through TGF $\beta$  receptor complex, leading to Smad2/3 phosphorylation and translocation to the nucleus, where it activates the promoters of genes that encode the ECM proteins and *Acta2*.<sup>12</sup> TWEAK

(P and Q) Representative immunoblots (P) and quantification (Q) of L524-0366 and vehicle control-treated mouse lung lysates on day 14.  $\beta$ -Actin is a loading control for whole-lung lysates. Saline/vehicle,  $n = 2$  mice; saline/L524-0366,  $n = 2$  mice; bleo/vehicle,  $n = 11$  mice; bleo/L524-0366,  $n = 10$  mice. Data in (A), (C)–(H), (J), (K), (M)–(O), and (Q) represent mean  $\pm$  SEM. Similar results were seen in at least three independent experiments.  $p$  value is calculated using the following: (A), (F), and (K), two-tailed t test; (B) and (L), log-rank test; (C)–(E), (G), (H), (J), (M)–(O), and (Q), two-way ANOVA. \*\*\* $p < 0.0001$ , \*\* $p < 0.001$ , \* $p < 0.01$ , \* $p < 0.05$ . NS, not significant. See also Figure S2–S4.

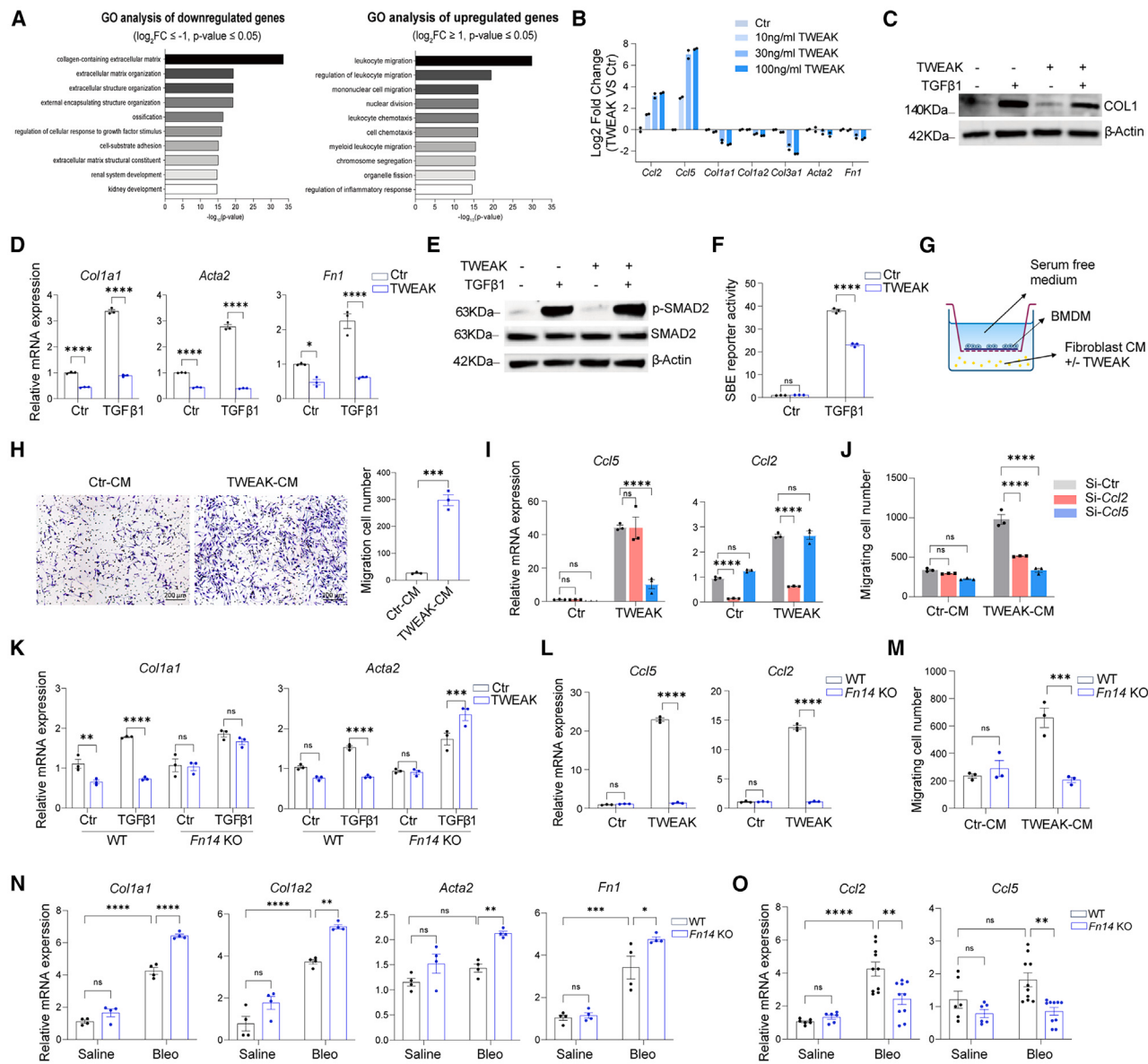


**Figure 3. TWEAK-Fn14 signaling inhibits fibrotic gene expression and induces chemokine expression in lung fibroblasts**

- (A) Top 20 GO biological processes enriched in the 1,251 downregulated genes ( $\log_2 \text{FC} \leq -1$ ,  $p$  value  $\leq 0.05$ ) and top 20 GO biological processes enriched in the 1,366 upregulated genes ( $\log_2 \text{FC} \geq 1$ ,  $p$  value  $\leq 0.05$ ) in MLFs treated with 30 ng/mL TWEAK for 48 h.
- (B) Chemokine and fibrotic gene expression in MLFs treated with 10, 30, and 100 ng/mL TWEAK for 48 h.
- (C and D) Representative immunoblots (C) and fibrotic gene expression (D) in MLFs treated with 30 ng/mL TWEAK and/or 4 ng/mL TGF $\beta$ 1 for 48 h.  $\beta$ -Actin is a loading control for whole-cell lysates.  $n = 3$  biological replicates.
- (E) Representative immunoblots of MLFs treated with 30 ng/mL TWEAK and/or 4 ng/mL TGF $\beta$ 1 for 2 h.  $\beta$ -Actin is a loading control for whole-cell lysates.
- (F) SBE reporter activity of HEK293T treated with 30 ng/mL TWEAK and/or 4 ng/mL TGF $\beta$ 1 for 6 h,  $n = 3$  biological replicates.
- (G) Schematic diagram of Transwell migration assay.
- (H) Representative images (left) and quantification (right) of macrophage migration induced by TWEAK-CM for 16 h,  $n = 3$  biological replicates. Scale bar, 200  $\mu$ m.
- (I) Chemokine expression in MLFs transfected with Ccl2, Ccl5 or control siRNA in the presence or absence of 30 ng/mL TWEAK,  $n = 3$  biological replicates.
- (J) Quantification of macrophage migration induced by CM from fibroblasts transfected with Ccl2, Ccl5, or control siRNA in the presence or absence of TWEAK,  $n = 3$  biological replicates.
- (K) Fibrotic gene expression of WT and Fn14-KO MLFs in the presence of 30 ng/mL TWEAK and/or 4 ng/mL TGF $\beta$ 1,  $n = 3$  biological replicates.
- (L) Chemokine expression of WT and Fn14-KO MLF in the presence of 30 ng/mL TWEAK,  $n = 3$  biological replicates.
- (M) Quantification of macrophage migration induced by TWEAK-stimulated WT and Fn14-KO fibroblast CM for 16 h,  $n = 3$  biological replicates.
- (N) Relative mRNA levels of Col1a1, Col1a2, Acta2, and Fn1 in the lung fibroblasts isolated from WT and Fn14-KO mice 7 days post bleomycin,  $n = 4$  biological replicates.

(legend continued on next page)

did not affect TGF $\beta$ 1-induced Smad2 phosphorylation (Figure 3E), but decreased TGF $\beta$ -responsive Smad-binding element (SBE) reporter activity (Figure 3F). These results showed that TWEAK antagonizes TGF $\beta$ /Smad signaling in MLFs, leading to inhibition of fibroblast activation and ECM synthesis.

Among the upregulated DEGs ( $\log_2\text{FC} \geq 1, p \text{ value} \leq 0.05$ ) in the RNA-seq of TWEAK-treated lung fibroblasts, “leukocyte migration” was the most strongly enriched GO term (Figure 3A), which is consistent with the previously reported role of TWEAK signaling in inducing proinflammatory responses and leukocyte infiltration.<sup>24–26</sup> The expression of chemokines such as *Ccl2* and *Ccl5* was upregulated in a dose-dependent manner in MLFs (Figure 3B). *Ccl2* is required for monocyte trafficking into the lung.<sup>44</sup> *Ccl5* is a potent chemoattractant cytokine to recruit monocytes and T cells into the lung<sup>45</sup> and can induce migration of bone-marrow-derived macrophages (BMDM) (Figure S6A). To test whether TWEAK signaling is able to recruit monocytes/macrophages, we collected the conditioned medium (CM) from MLFs after TWEAK stimulation. TWEAK-CM induced chemotaxis of BMDM (Figures 3G and 3H), though TWEAK itself had no effect (Figure S6A). Knocking down *Ccl2* or *Ccl5* in fibroblasts using small interfering RNA (siRNA) blocked TWEAK-CM-induced BMDM migration (Figures 3I and 3J), suggesting fibroblasts secrete chemokines to recruit macrophages in response to TWEAK stimulation.

TWEAK-Fn14 signaling has been reported to activate both the canonical NF- $\kappa$ B signaling pathway, leading to RelA (also known as p65) activation, and noncanonical NF- $\kappa$ B signaling, involving processing of p100 to p52.<sup>46–48</sup> Kyoto Encyclopedia of Genes and Genomes (KEGG) analysis of the RNA-seq data showed that TNF and NF- $\kappa$ B signaling pathways were among the top upregulated pathways induced by TWEAK (Figure S6B). As expected, TWEAK stimulation robustly induced RelA phosphorylation and p100 processing to p52 (Figure S6C). We then examined whether NF- $\kappa$ B signaling is required for TWEAK-induced ECM inhibition and chemokine expression. Knocking down *Rela* or *Relb* in fibroblasts using siRNA significantly reduced TWEAK-induced chemokine expression but had no effects on ECM gene expression (Figure S6D–S6F), suggesting TWEAK-induced chemokine expression is dependent on NF- $\kappa$ B signaling, whereas TGF $\beta$ /Smad signaling antagonization is independent of NF- $\kappa$ B signaling.

Next, we asked whether TWEAK’s effect on lung fibroblasts is mediated by Fn14. We flow sorted primary MLFs from WT and *Fn14*-KO mice. Recombinant TWEAK protein failed to inhibit ECM gene expression or induce *Ccl2* or *Ccl5* expression in the *Fn14*-KO fibroblasts (Figures 3K and 3L). Consistently, TWEAK-CM from *Fn14*-KO lung fibroblasts cannot induce BMDM migration (Figure 3M). These data confirmed that Fn14 is the receptor mediating TWEAK function in lung fibroblasts.

To explore whether similar mechanisms happened *in vivo*, we isolated primary MLFs from WT and *Fn14*-KO mice at day 7 post bleomycin injury and analyzed the gene expression by qPCR.

The expression of ECM genes and *Acta2* was increased in the *Fn14*-KO fibroblasts, whereas *Ccl2* and *Ccl5* were decreased (Figures 3N and 3O), consistent with the results observed in cultured cells.

To further examine whether TWEAK has similar roles in human lung fibroblasts (HLFs), we extended our findings to primary HLFs from both healthy donors and IPF patients. In agreement with the results observed in MLFs, we found that in normal HLFs, TWEAK inhibited fibroblast activation and ECM gene expression at both baseline and after TGF $\beta$ 1 stimulation and induced *CCL5* expression (Figure S7A–S7C). TWEAK also inhibited ECM production and increased *CCL5* expression in IPF lung fibroblasts (IPF HLF) in a dose-dependent manner (Figure S7C and S7D). To demonstrate that TWEAK’s effect is dependent on Fn14 in human lungs, we treated normal HLF with Fn14 antagonist L524-0366 and found that TWEAK failed to inhibit ECM gene expression or induce *CCL5* expression in the presence of L524-0366 (Figure S7E). TWEAK had no effects on the proliferation or migration of HLFs (Figure S7F–S7H). These results collectively demonstrated that TWEAK inhibits fibroblast activation and ECM synthesis and induces chemokine expression in both mouse and HLFs.

#### ***Fn14* deficiency impairs macrophage infiltration and differentiation in the lung**

Next, we explored whether *Fn14* deficiency affects immune cell infiltration in the lung. All the immune cells (CD45 $^+$  EPCAM $^-$  CD31 $^-$ ) from WT and *Fn14*-KO mice 7 and 14 days post bleomycin injury were sorted and sequenced using 10x Genomics Chromium platform (Figure 4A). A single-cell transcriptome of 52,437 cells after quality control filtering were visualized using the Uniform Manifold Approximation and Projection (UMAP).<sup>49</sup> Using canonical lineage-defining markers to annotate the clusters (Figure S8A), we defined seven cell types, including macrophages, monocytes, dendritic cells (DCs), natural killer (NK) cells, neutrophils, B cells, and T cells (Figure 4B). After bleomycin injury, the immune cell composition changed as expected, including the percentage of macrophages in total immune cells increased at day 7, and then decreased at day 14 (Figure 4C). Compared with WT mice, *Fn14* KO reduced macrophages at both 7 and 14 days post bleomycin injury without obvious impacts on other immune cell types (Figure 4C), indicating *Fn14* deficiency impairs macrophage recruitment into the lung.

Macrophages in the lungs are classified as alveolar macrophages (AMs) or interstitial macrophages (IMs) based on their localization.<sup>50</sup> During the inflammatory phase following bleomycin injury, the number of AMs significantly decreases whereas the number of IMs increases.<sup>17,51</sup> Monocytes are recruited to the lung and differentiate into macrophages, replenishing the AM pool.<sup>6</sup> The CCL2-CCR2 axis is responsible for monocyte recruitment into the lung and depleting circulating monocytes using *Ccr2* $^{-/-}$  mice ameliorates fibrosis severity.<sup>52,53</sup> Monocyte-derived alveolar macrophages (Mo-AMs) are reported to

(O) Relative mRNA levels of chemokine genes *Ccl2* and *Ccl5* in the lung fibroblasts isolated from WT and *Fn14*-KO mice 7 days post bleomycin. Saline,  $n = 6$  biological replicates/group; bleo,  $n = 10$  biological replicates/group. Data in (D), (F), (H)–(O) represent mean  $\pm$  SEM. Similar results were seen in at least three independent experiments.  $p$  value is calculated using the following: (D), (F), and (I)–(O), two-way ANOVA; (H), two-tailed t test. \*\*\* $p < 0.0001$ , \*\* $p < 0.001$ , \* $p < 0.01$ , \* $p < 0.05$ . NS, not significant. See also Figure S5–S7.

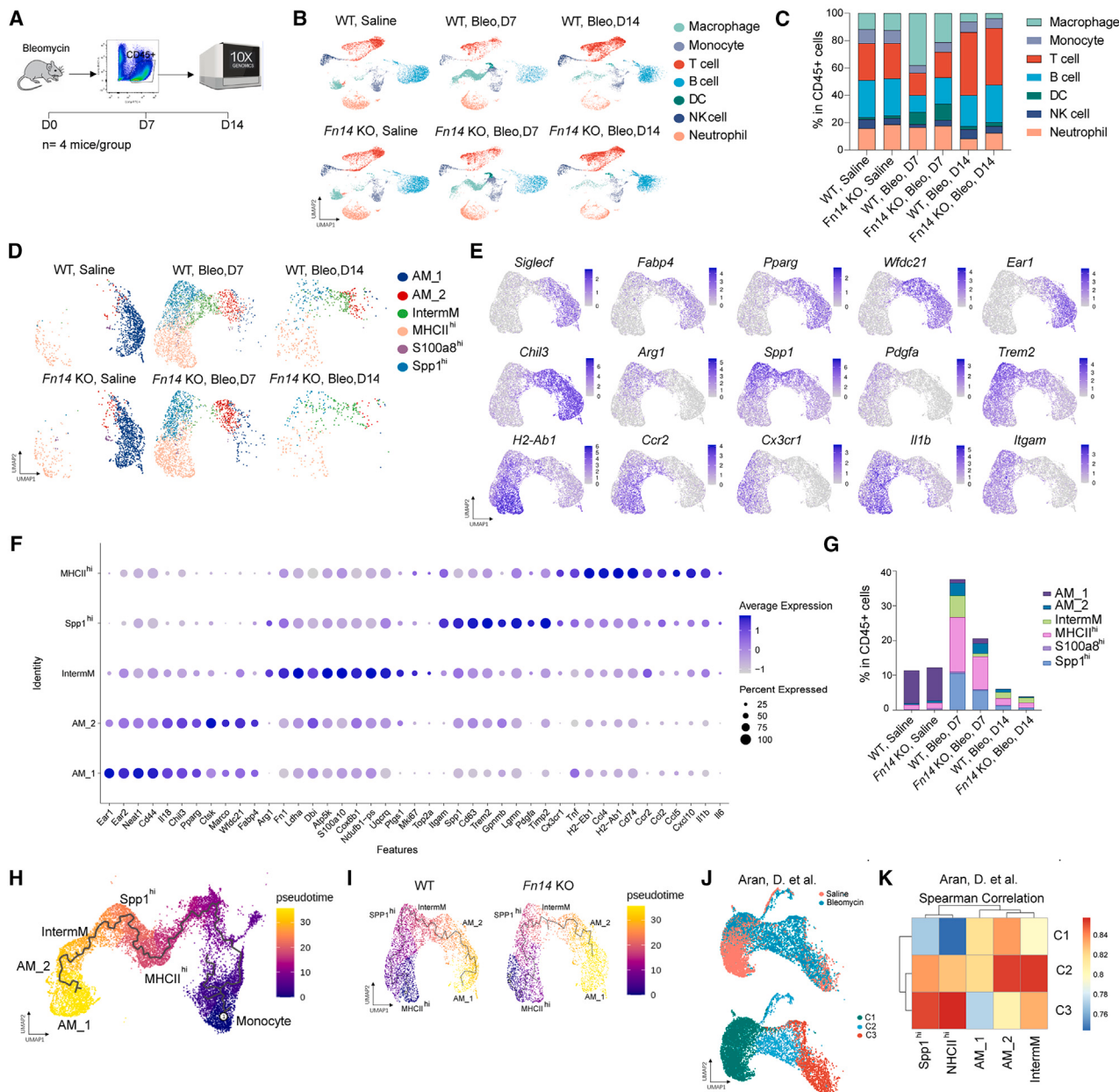


**Figure 4. Fn14 deficiency reduces macrophage recruitment after bleomycin injury**

- (A) Schematic diagram of scRNA-seq experiment,  $n = 4$  mice per group.
- (B) UMAP representation of 52437 Cd45<sup>+</sup> cells from WT and Fn14-KO lungs in saline and bleomycin groups, each dot represents a single cell.
- (C) Percentage of individual cell types in all CD45<sup>+</sup> cells.
- (D) UMAP representation of 7,850 macrophages from WT and Fn14-KO lungs in saline and bleomycin groups, each dot represents a single cell.
- (E) UMAP representation of gene expression in each distinct subcluster.
- (F) Dotplot of gene expression in each distinct subcluster.
- (G) Percentage of macrophages subpopulations in all CD45<sup>+</sup> cells.
- (H and I) Monocle3-based pseudotime analysis of all the monocytes and macrophages (H) and macrophages only in WT and Fn14-KO lungs (I).
- (J) UMAP of macrophages from the published scRNA-seq results of bleomycin-injured lungs on day 14.<sup>18</sup>
- (K) Spearman correlation coefficients of single-cell transcriptomic profiles between our study and published dataset<sup>18</sup> based on the top 2,000 most variable genes.

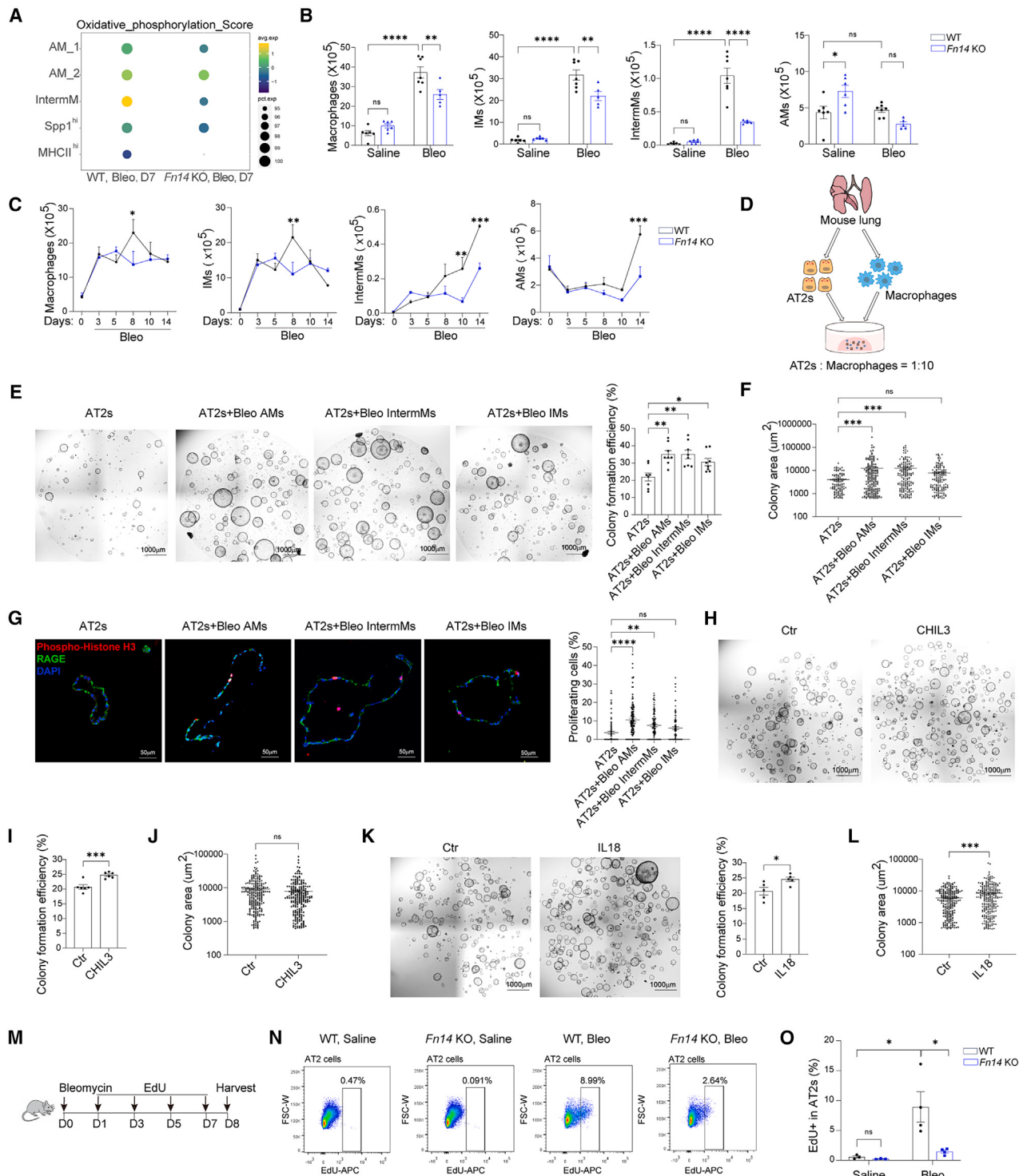


**Figure 5. Fn14 deficiency diminishes a macrophage subpopulation that may promote alveolar regeneration after bleomycin injury**

(A) Dotplot of oxidative phosphorylation score in different macrophage subpopulations.

(B) Quantification of macrophage cell counts by flow cytometry in the WT and Fn14-KO lungs 7 days post bleomycin. Saline/WT,  $n = 6$  mice; saline/KO,  $n = 6$  mice; bleo/WT,  $n = 7$  mice; bleo/KO,  $n = 5$  mice.

(C) Quantification of macrophage cell counts by flow cytometry in the WT and Fn14-KO lungs 3/5/8/10/14 days post bleomycin.  $n = 3$  mice in each group.

(D) Schematic diagram of 3D organoid co-cultures of AT2 and macrophages.

(legend continued on next page)

drive lung fibrosis in the bleomycin model.<sup>13</sup> However, CCR2<sup>+</sup> monocyte-derived macrophages are shown to promote alveolar regeneration after pneumectomy.<sup>15</sup> Distinct CCR2<sup>+</sup> macrophage subpopulations may exist and execute different functions in fibrosis and regeneration.

To determine the subpopulations recruited by TWEAK-Fn14 signaling, we subclustered the macrophages into six distinct cell clusters (Figure 4D, Table S2). AM\_1 was predominantly from saline controls, highly expressing AM markers *Ear1*, *Ear2*, *Chil3*, *Pparg*, and *Iil8*, and replaced by AM\_2 post injury (Figures 4D–4F). MHCII<sup>high</sup> IMs were the interstitial macrophages in the saline lungs and significantly expanded 7 days after injury. MHCII<sup>high</sup> IMs highly expressed MHCII genes, *Tnf*, *Iilb*, *Cx3cr1*, *Ccr2*, and chemokines, suggesting a proinflammatory role (Figures 4E and 4F). SPP1<sup>high</sup> IMs emerged after injury and were characterized by expression of *Spp1*, *Trem2*, *Lgmn*, *Pdgfa*, and *Timp2* (Figures 4D–4F), reminiscent of SPP1<sup>+</sup> CD163<sup>+</sup> profibrotic macrophages in human IPF lungs.<sup>20–22</sup> S100a8<sup>hi</sup> IMs were dispersed, small in quantity, and high in expression of apoptotic markers, for example *Mmp9*,<sup>54</sup> *Pglyrp1*,<sup>55</sup> *Lcn2*,<sup>56</sup> and *G0s2*,<sup>57</sup> indicating apoptotic cells (Figure 4D and S8B).

AMs are identified as CD11c<sup>+</sup> CD11b<sup>−</sup> SiglecF<sup>+</sup> MHCII<sup>lo</sup>, whereas IMs are CD11b<sup>+</sup> SiglecF<sup>−</sup>, as previously described.<sup>18,58</sup> In-between AMs and IMs, there was an intermediate macrophage subpopulation (termed as IntermMs) sharing the features of both AMs and IMs, characterized by CD11b<sup>−</sup> SiglecF<sup>−</sup> MHCII<sup>lo</sup> (Figures 4E and 4F). This subpopulation expressed *Ccr2*, indicative of monocytic origin, but had lower expression of *Cx3cr1*, *Iil6*, *Tnf*, and *Itgam* compared with IMs. They expressed *Cox6b1*, which is implicated in reducing ROS production,<sup>59</sup> and *s100a10*, which can promote macrophage migration.<sup>60</sup> They also highly expressed *Arg1*, *Fn14*, *Mki67*, and *Top2a*, suggesting proliferating macrophages (Figures 4E and 4F).

In *Fn14*-KO mice, all of the six macrophage subpopulations were decreased at day 7 and day 14 compared with WT mice (Figure 4G), suggesting *Fn14* deficiency impairs macrophage infiltration in the lung. The most dramatic loss was observed in the IntermMs (Figure 4G). In order to understand the cell of origin of IntermMs, we pooled together monocytes and macrophages of WT or *Fn14*-KO mice and did pseudo time analysis using Monocle 3,<sup>61,62</sup> which predicted a trajectory from monocytes toward MHCII<sup>high</sup> IMs, SPP1<sup>high</sup> IMs, IntermMs, and then AMs, suggesting a continuous transition path (Figure 4H), consistent with the previously reported monocyte to AM differentiation.<sup>10,22</sup>

Furthermore, this transition seemed to be impaired in *Fn14*-KO mice compared with WT mice, as by day 14 there were fewer AM\_2 in the KO group (Figures 4G and 4I). Collectively, these data suggest that *Fn14* deficiency attenuates macrophage recruitment in the lung and affects the differentiation of monocytes to AMs.

Previously, scRNA-seq analysis of bleomycin-injured lungs at day 14 revealed three distinct macrophage subclusters, including AMs (cluster C1), IMs (cluster C3), and a transitional cluster (C2) intermediate between monocyte-derived and AMs.<sup>18</sup> We thus compared the transcriptional similarity between the macrophage subpopulations identified in our study and the published study. We found IntermMs and AM\_2 closely resemble C2, while MHCII<sup>high</sup> IMs and SPP1<sup>high</sup> IMs are more similar to C3 (Figures 4J and 4K and S9), confirming IntermM is intermediate between monocyte-derived and AMs. Of note, Clusters C2 and C3 have been shown to promote fibrosis by secreting platelet-derived growth factor subunit A (PDGFA).<sup>18</sup> However, IntermMs and AM\_2, though transcriptionally resemble C2, had lower expression of PDGFA and CX3CR1 expression compared with SPP1<sup>high</sup> IMs (Figure 4F).

### The IntermMs and AMs emerging after bleomycin injury have the capability to promote alveolar regeneration

Next, we explored the role of IntermMs in alveolar regeneration and fibrogenesis. GO analysis of DEGs among the macrophage subpopulations revealed that “mitochondrial respirasome” and “oxidative phosphorylation (OXPHOS)” were the top GOs enriched in the upregulated genes of IntermMs (Figure S10A). OXPHOS score in IntermMs was higher than that in all other macrophage subpopulations and was decreased in *Fn14*-KO mice (Figure 5A). Increased OXPHOS in macrophages has been linked to reduced inflammation and promotion of tissue repair.<sup>63,64</sup> According to previous reports, CCR2<sup>+</sup> monocytes and Arg1<sup>+</sup> macrophages<sup>13</sup> as well as IMs<sup>15</sup> can promote alveolar regeneration. Thus, we reasoned the IntermMs may have a regenerative role. To test this hypothesis, we flow sorted IntermMs (CD64<sup>+</sup> CD11c<sup>+</sup> CD11b<sup>−</sup> SiglecF<sup>−</sup>) together with AMs (CD64<sup>+</sup> CD11c<sup>+</sup> CD11b<sup>−</sup> SiglecF<sup>+</sup>) and IMs (CD64<sup>+</sup> CD11b<sup>+</sup> SiglecF<sup>−</sup>) using the surface markers identified by our scRNA-seq data and the previously reported sorting strategy for macrophages<sup>65</sup> (Figure S10B and S10C).

IM, IntermM, and total macrophage cell numbers were all increased in WT mice 7 days after bleomycin injury and

- (E) Representative images (left) and quantification (right) of mouse AT2 organoid after 10-day co-culture with macrophages,  $n = 8$  droplets/group. Scale bar, 1,000  $\mu\text{m}$ .
- (F) Colony size of mouse AT2 organoids co-cultured with macrophages,  $n = 3$  droplets with over 200 organoids.
- (G) Representative images of immunofluorescence staining (left) and quantification (right) of proliferating AT2 cells in the organoids. Each data point represents a colony.  $n > 100$  colonies in each group. The proliferation marker phospho-Histone H3 (red), AT1 marker RAGE (green), DAPI (blue). Scale bar, 50  $\mu\text{m}$ .
- (H and I) Representative images (H) and quantification (I) of mouse AT2 organoids treated with 200 ng/mL CHIL3,  $n = 6$  droplets/group. Scale bar, 1,000  $\mu\text{m}$ .
- (J) Colony size of mouse AT2 organoids treated with CHIL3,  $n = 3$  droplets with over 200 organoids.
- (K) Representative images (right) and quantification (left) of mouse AT2 organoids treated with 200 ng/mL IL-18,  $n = 5$  droplets/group. Scale bar, 1,000  $\mu\text{m}$ .
- (L) Colony size of mouse AT2 organoids treated with IL-18,  $n = 3$  droplets with over 200 organoids.
- (M) Schematic diagram of EdU incorporation experiment.
- (N) Representative flow cytometry plots showing gating strategy used for identification of EdU<sup>+</sup> AT2s in mouse lungs.
- (O) Percentage of proliferating AT2 cells in all the AT2s measured by FACS. Saline,  $n = 3$  mice/group; bleo,  $n = 4$  mice/group. Data in (B), (C), (E)–(G), (I)–(L), and (O) represent mean  $\pm$  SEM. Similar results were seen in at least three independent experiments.  $p$  value is calculated using the following: (B), (C), and (O), two-way ANOVA; (E)–(G), one-way ANOVA; (I)–(L), two-tailed t test. \*\*\* $p < 0.0001$ , \*\* $p < 0.001$ , \* $p < 0.05$ . NS, not significant. See also Figure S8–S10.

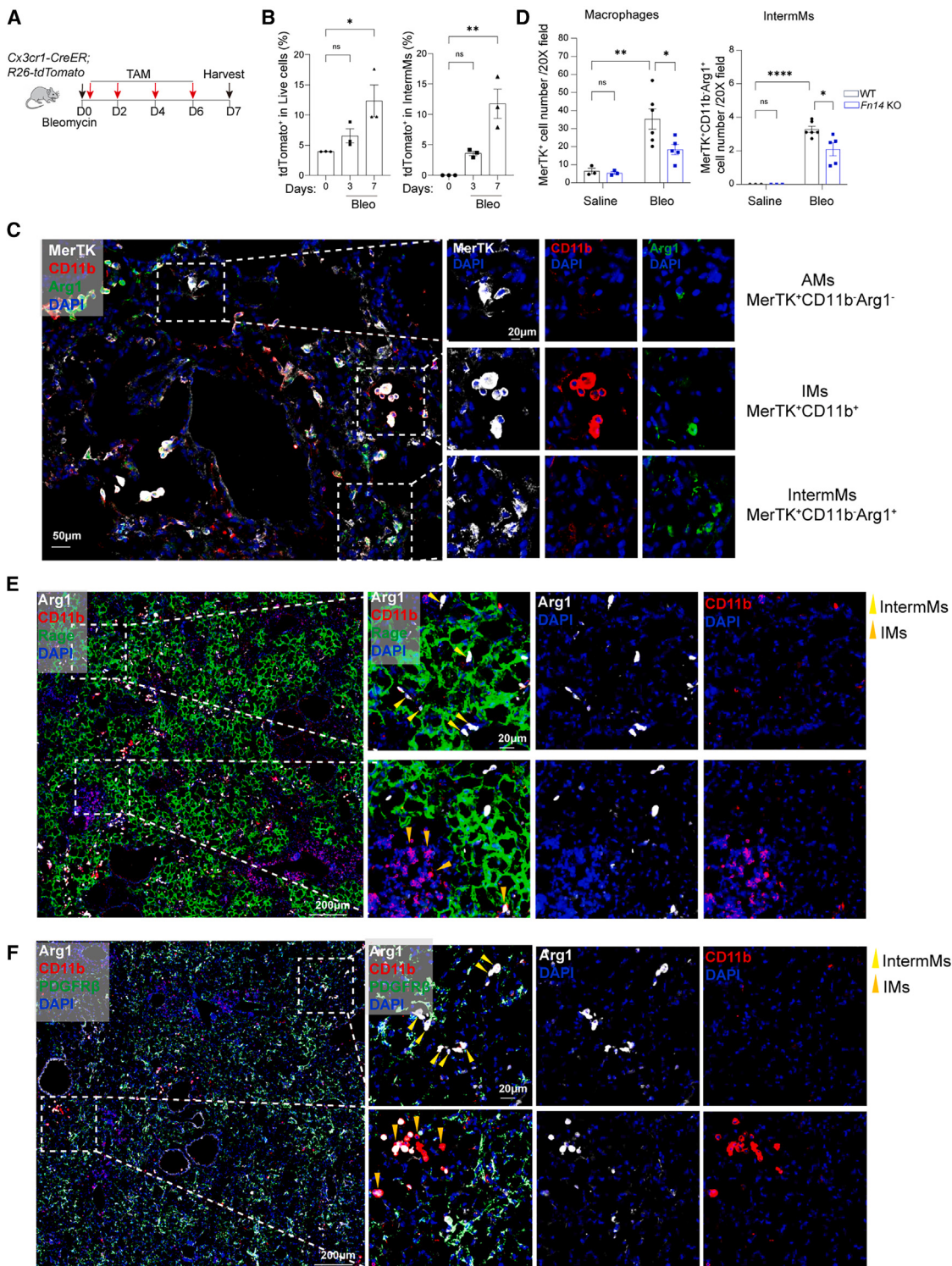


**Figure 6. The localization of InterMs in the fibrotic lungs**

(A) Schematic diagram of Cx3cr1-CreER; R26-tdTomato mice lineage tracing in bleomycin model.

(B) Flow cytometry analysis of tdTomato+ cells in macrophages post bleomycin injury.  $n = 3$  mice in each group.

(legend continued on next page)

significantly decreased in *Fn14*-KO mice (Figure 5B and S10D), confirming *Fn14* deficiency impairs macrophage recruitment into the lung. To explore the dynamic changes of macrophage subpopulations, we examined the subpopulations at multiple timepoints after bleomycin (day 3, 5, 8, 10, and 14). Consistent with the scRNA-seq results, the total number of macrophages increased after injury, peaking on day 8 before declining on days 10 and 14. IMs exhibited a similar trend, while AMs decreased by day 3 and then increased by day 14. In contrast, IntermMs continued to rise after injury (Figure 5C). In *Fn14*-KO mice, all the subpopulations were decreased on day 8, but by day 14, there were fewer AMs and IntermMs while more IMs, suggesting *Fn14* KO inhibits both macrophage recruitment and differentiation toward AMs.

Then we examined the role of macrophage subpopulations in alveolar organoid cultures (Figure 5D). When coculturing AT2s with AMs and IMs from saline controls, both macrophage populations lead to more and larger organoid formation, with IMs more potent than AMs (Figure S10E and S10F), which is consistent with a previous report.<sup>17</sup> After bleomycin injury, both IntermMs and AMs significantly increased colony number and size, whereas IMs had no significant effects on colony size, despite increasing colony formation (Figures 5E and 5F). Moreover, we examined AT2 cell proliferation by immunofluorescence staining for phosphor-Histone H3. Both IntermMs and AMs induced AT2 proliferation, whereas IMs had no significant effects (Figure 5G), suggesting IntermMs and AMs acquire more potent pro-regenerative capacity than IMs.

To understand how IntermMs and AMs promote AT2 proliferation, we analyzed the scRNA-seq data to explore the genes that encode secreted factors shared between IntermMs and AMs and noticed chitinase-like protein 3 (CHIL3) and interleukin 18 (IL-18) were enriched in IntermMs and AMs (Figure 4F). CHIL3 has been reported to stimulate neural stem cell self-renewal as a niche factor.<sup>66</sup> IL-18 is a member of the IL-1 family of cytokines, among which IL-1 $\alpha/\beta$  has been reported to promote AT2 proliferation.<sup>17,67</sup> Both CHIL3 and IL-18 treatment significantly increased the colony formation efficiency (Figures 5H–5J), and IL-18 increased the colony size of AT2 organoids (Figures 5K and 5L), suggesting IntermMs and AMs may secret cytokines like CHIL3 and IL-18 to induce AT2 proliferation. In summary, injury-induced IntermMs together with AMs are capable of promoting AT2 proliferation.

To validate whether *Fn14* deficiency impairs alveolar regeneration *in vivo*, we examined AT2 proliferation after bleomycin injury (Figure 5M). Flow cytometry showed that the proliferating AT2s were significantly decreased in the *Fn14*-KO mice (Figures 5N and 5O). Taken together, both *in vitro* and *in vivo* studies collectively support that TWEAK-*Fn14* signaling promotes macrophage recruitment and differentiation in the lung, leading to alveolar regeneration.

Next, we explored the ontogeny of IntermMs. *Cx3cr1-CreER; Rosa26-LSL-tdTomato* mice were used to trace monocytes following previously described methods.<sup>18</sup> We observed about 4% of live cells were tdTomato<sup>+</sup> at baseline, consistent with the previous report.<sup>18</sup> Bleomycin injury induced an increase of tdTomato<sup>+</sup> cells in both total lung cells and IntermMs (Figures 6A and 6B), suggesting IntermMs are monocyte-derived macrophages.

We then examined the tissue localization of IntermMs. Based on the scRNA-seq results (Figure 4F), we established an immunofluorescence staining panel to distinguish the macrophage subpopulations in the lung, with AMs stained as MerTK<sup>+</sup> CD11b<sup>−</sup> Arg1<sup>−</sup>, IMs as MerTK<sup>+</sup> CD11b<sup>+</sup>, and IntermMs as MerTK<sup>+</sup> CD11b<sup>−</sup> Arg1<sup>+</sup> (Figure 6C). The quantification of immunofluorescence staining confirmed that *Fn14* deficiency decreased total macrophage number and IntermM number at day 7 post bleomycin (Figure 6D). We then co-stained macrophage markers with AT1 and fibroblast markers to determine the spatial organization of IntermMs. IntermMs were detected in direct contact with or adjacent to Rage<sup>+</sup> AT1s or PDGFR $\beta$ + fibroblasts in the alveolar regions, while IMs were found in clusters separated from AT1s or PDGFR $\beta$ + fibroblasts (Figures 6E and 6F), suggesting IntermMs and IMs are in distinct anatomical locations.

### InterM subpopulation exists in human fibrotic lungs

To further evaluate our findings, we reanalyzed the scRNA-seq data from IPF and normal human lungs (GEO: GSE135893)<sup>34</sup> and assessed whether the IntermM subpopulation exists in human fibrotic lungs. Macrophages were clustered into four subpopulations based on reported markers<sup>68</sup> (Figures 7A and 7B). FABP4<sup>high</sup> macrophages were decreased in IPF lungs, whereas SPP1<sup>high</sup> macrophages, FCN1<sup>high</sup> macrophages, and a proliferating macrophage population were increased in IPF lungs. FABP4<sup>high</sup> macrophages were defined by high expression of FABP4, INHBA, and MARCO, characteristic of AMs (Figure 7C). FCN1<sup>high</sup> macrophages highly express FCN1 and IL1B, suggesting a proinflammatory role; while SPP1<sup>high</sup> macrophages highly express SPP1 and MERTK, consistent with previously identified profibrotic macrophages.<sup>19–22</sup> There was a proliferating macrophage population, characterized by expression of MK67 and TOP2A. These proliferating macrophages share highly similar transcriptional profiles with IntermMs (Figure 7D). Furthermore, pseudotime analysis predicted a trajectory from FCN1<sup>high</sup> macrophages toward SPP1<sup>high</sup> macrophages, proliferating macrophages, then FABP4<sup>high</sup> AMs (Figure 7E), similar to the monocyte to AM differentiation in mouse lungs.

We then asked whether *Fn14* upregulation and the IntermM subpopulation exists in other types of pulmonary fibrosis (PF). In the same dataset (GEO: GSE135893),<sup>34</sup> there were explanted fibrotic lungs from patients with chronic hypersensitivity

(C and D) Representative immunofluorescence images (C) and quantification (D) of macrophage subpopulations in the WT and *Fn14*-KO lungs 7 days post bleomycin. MerTK (white), CD11b (red), Arg1 (green), DAPI (blue). Saline/WT, n = 3 mice; saline/KO, n = 3 mice; bleo/WT, n = 6 mice; bleo/KO, n = 5 mice. Scale bar, 50  $\mu$ m, 20  $\mu$ m.

(E and F) Representative immunofluorescence images of IntermMs and IMs 14 days after bleomycin injury. AT1 marker Rage (green) (E), fibroblast marker PDGFR $\beta$  (green) (F), Arg1 (white), CD11b (red), DAPI (blue). Yellow arrows: IntermMs; orange arrows: IMs. Scale bar, 200  $\mu$ m, 20  $\mu$ m. Data in (B) and (D) represent mean  $\pm$  SEM. p value is calculated using the following: (B), one-way ANOVA; (D), two-way ANOVA. \*\*\*p < 0.0001, \*\*p < 0.01, \*p < 0.05. NS, not significant.

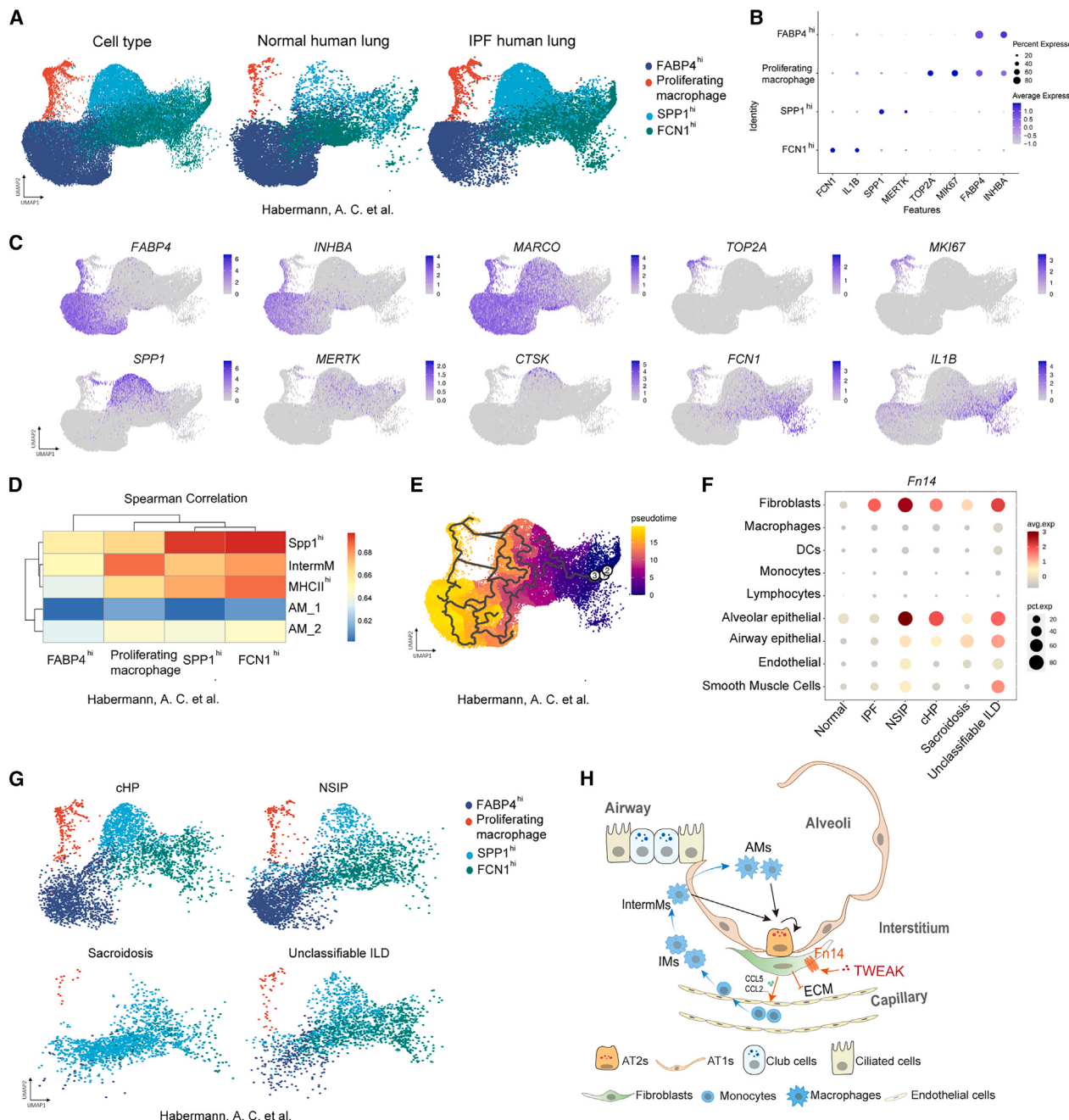


**Figure 7. InterMs resemble the proliferating macrophages in IPF lungs**

(A) UMAP representation of macrophages in normal lung and IPF lung.<sup>34</sup>

(B) Cellular markers that classify normal and IPF human lung macrophages.

(C) UMAP representation of gene expression of key markers in each distinct subcluster.

(D) Spearman correlation coefficients of single-cell transcriptomic profiles between our study and published dataset<sup>34</sup> based on the top 2,000 most variable genes.

(E) Monocle3-based pseudotime analysis of human lung macrophages.

(F and G) Dotplot of Fn14 expression (F) and UMAP representation of macrophages and proliferating macrophages (G) in normal lung, IPF, cHP, NSIP, sarcoidosis, and unclassifiable ILD.

(H) Schematic summary of the role of TWEAK-Fn14 signaling in pulmonary fibrosis. TWEAK inhibits fibroblast activation and ECM production via its receptor Fn14 in the fibroblasts. On the other hand, TWEAK-Fn14 induces chemokine in fibroblasts to recruit monocytes into the lung and activate monocyte differentiation to InterMs and AMs, which promote AT2 proliferation and thus alveolar regeneration. See also Figure S11.

pneumonitis (cHP), nonspecific interstitial pneumonia (NSIP), sarcoidosis, and unclassifiable ILD. We analyzed the scRNA-seq results from these conditions and found in all of them, Fn14 expression was upregulated in the fibroblasts, though Fn14 expression in other cell types varied (Figure 7F), and proliferating macrophages, reminiscent of IntermMs, exist in all of these conditions (Figure 7G). These data collectively showed that in both mouse and human fibrotic lungs, there is Fn14 upregulation in fibroblasts and an intermediate macrophage population between IMs and AMs.

## DISCUSSION

Fibroblast-macrophage reciprocal interactions play important roles in fibrosis.<sup>6–8</sup> Here, our study demonstrated that TWEAK-Fn14 signaling mediates crosstalk between fibroblasts and macrophages to play a protective role against lung fibrosis. Fn14, whose expression is typically low in healthy tissues,<sup>24,35</sup> is robustly induced in (myo)fibroblasts by proinflammatory signals in fibrotic lungs. TWEAK-Fn14 signaling inhibits TGF $\beta$  signaling and ECM synthesis in fibroblasts, leading to attenuation of fibrosis as negative feedback. Meanwhile, TWEAK-Fn14 signaling induces chemokine expression via NF- $\kappa$ B signaling to recruit monocytes/macrophages into the lung (Figure 7H). Furthermore, single-cell transcriptomics of *Fn14*-KO mice allowed us to identify an injury-induced transitional macrophage subpopulation termed IntermMs, which is able to promote alveolar regeneration at a similar extent as AMs and is largely diminished in *Fn14*-KO mice.

The role of macrophages in lung fibrosis is complicated and context dependent. Although multiple studies have reported profibrotic monocyte-derived macrophage subpopulations,<sup>18–23</sup> macrophages are also implicated in the resolution of fibrosis and tissue repair.<sup>15,23,69</sup> By comparing the macrophage subpopulations in WT and *Fn14*-KO mice, we identified an IntermM subpopulation, which shares the transcriptional similarity with the previously described transitional subpopulation C2<sup>18</sup> and represents a transitional state that may eventually differentiate into AMs to replenish the depleted AMs, consistent with the previously reported role for EGR2-dependent monocyte-derived AMs in tissue repair.<sup>69</sup> Our results indicate that during monocyte to AM differentiation, macrophage subpopulations probably transit from proinflammatory (MHCII<sup>high</sup> IMs) or profibrotic (SPP1<sup>high</sup> IMs) function to pro-regenerative (IntermMs, AMs) function, though it is not clear whether IMs and AMs originate from the same monocyte population. These results highlight the plasticity and functional diversity of macrophage subpopulations after tissue injury. Interestingly, transcriptional similarity and pseudotime analysis of IPF lungs predicted similar macrophage subpopulations and transition paths exist in human fibrotic lungs.

AMs and IMs are exposed to different environments, thus displaying distinctive metabolic profiles. AMs are in low-glucose and high lipid-rich surfactant environment, thus express elevated levels of PPAR $\gamma$  and genes associated with lipid metabolism, and reduced expression of genes associated with glycolysis.<sup>70,71</sup> In contrast to AMs, IMs residing in the lung tissue appear much more glycolytically active than their AM counter-

parts.<sup>58</sup> High PPAR $\gamma$  expression (Figures 4E and 4F) and high rates of OXPHOS (Figure 5A) again suggest IntermMs represent a transitional state between IMs and AMs.

The TWEAK-Fn14 axis has been reported to promote fibrosis in the liver, kidney, heart, and skin.<sup>26,27</sup> However, our study using Fn14 KO mice and Fn14 antagonist demonstrated a protective role of the TWEAK-Fn14 axis in a lung fibrosis model. Mechanically, TWEAK-Fn14 signaling seems to have tissue-specific effects on (myo)fibroblasts, including promoting proliferation but not activation in hepatic stellate cells,<sup>28</sup> inducing pericyte proliferation, migration, and differentiation into myofibroblasts in the kidney,<sup>27</sup> promoting fibroblast proliferation and migration in the heart,<sup>43</sup> and enhancing dermal fibroblast migration.<sup>72</sup> In the lung fibroblasts, we observed that TWEAK does not affect fibroblast proliferation or migration, but inhibits fibroblast activation by downregulating TGF $\beta$  signaling. It partially explains the protective role of TWEAK-Fn14 signaling in lung fibrosis.

On the other hand, TWEAK-Fn14 signaling activates NF- $\kappa$ B signaling, leading to tissue inflammation.<sup>24–26</sup> Our results demonstrated that TWEAK-Fn14 signaling induces monocyte/macrophage infiltration into the lung in an NF- $\kappa$ B-dependent manner. Monocytes, once recruited to the lung, can differentiate into IntermMs and AMs, which are able to promote alveolar epithelial cell proliferation. The role of TWEAK-Fn14 signaling in tissue repair and regeneration has been reported in multiple organs, including liver regeneration after partial hepatectomy in mice<sup>31,70</sup> and healing of burn wounds.<sup>72</sup> Interestingly, a clinical observation of systemic sclerosis (SSc) demonstrated elevated circulating TWEAK levels in patients with SSc are associated with a lower frequency of PF,<sup>73</sup> which is consistent with the protective role we identified in a preclinical lung fibrosis model.

Recently, distinct fibroblast subsets have been identified in the fibrotic lungs by scRNA-seq.<sup>74</sup> Inflammatory fibroblasts, characterized by chemokine expression and response to inflammatory cytokines, have been reported to derive from alveolar fibroblasts during the early stages of injury and become fibrotic fibroblasts (myofibroblasts) in response to TGF $\beta$  signaling.<sup>74</sup> Fn14 expression, though induced by IL-1 $\beta$  and TNF $\alpha$  after injury, is not restricted in inflammatory fibroblasts. Instead, Fn14 is induced in multiple fibroblast subsets including fibrotic fibroblasts, stress-activated fibroblasts, and proliferating fibroblasts in both the bleomycin model and IPF lungs (Figure S11). Whether Fn14 signaling executes different functions (inhibiting TGF $\beta$  signaling to limit fibroblast activation and activating NF- $\kappa$ B signaling to promote inflammatory response) in distinct subsets needs further investigation.

To summarize, our work using *Fn14*-KO mice demonstrated a protective role of TWEAK-Fn14 signaling in lung fibrosis. *Fn14* deficiency increased ECM production in (myo)fibroblasts, impaired macrophage infiltration in the lung, and diminished a pro-regenerative IntermM subpopulation, leading to impaired alveolar regeneration and exacerbated lung fibrosis.

## Limitations of the study

Our study raises several unanswered questions. (1) Our work showed that TWEAK-Fn14 signaling antagonizes TGF $\beta$  signaling, which is independent of NF- $\kappa$ B and downstream of Smad2 phosphorylation. How exactly TWEAK-Fn14 signaling inhibits

TGF $\beta$  signaling needs further studies. (2) We combined scRNA-seq analysis, flow cytometry, and AT2 organoid co-culture assay to demonstrate that injury-induced InterMs and AMs can promote AT2 cell proliferation. However, whether and how this population promotes alveolar regeneration *in vivo* after bleomycin injury remains unclear.

### RESOURCE AVAILABILITY

#### Lead contact

Further information and requests for resources and reagents should be directed to and will be fulfilled by the lead contact, Ying Xi ([xiying@shanghaitech.edu.cn](mailto:xiying@shanghaitech.edu.cn)).

#### Materials availability

All materials generated in this study are available from the [lead contact](#) upon request.

#### Data and code availability

Raw sequencing files for RNA-seq and scRNA-seq analysis have been deposited in the Gene Expression Omnibus (GEO) database: GSE262923 and GSE262928. The publicly available scRNA-seq data reanalyzed in this study are available in the GEO: GSE135893, GSE141259, GSE111664, and GSE210341. This paper does not report original code. Any additional information required to reanalyze the data reported in this paper is available from the [lead contact](#) upon request.

### ACKNOWLEDGMENTS

This work was supported by the National Key R&D Program of China (No. 2020YFA0710800), National Natural Science Foundation of China (No. 82070065 and 92268102), Major Project of Guangzhou National Laboratory (No. GZNL2023A01003), Shanghai Frontiers Science Center for Biomacromolecules and Precision Medicine at ShanghaiTech University, and ShanghaiTech University start-up funds to Y.X. and National Key R&D Program of China (No. 2020YFA0710800, 2021YFA0804703) and National Natural Science Foundation of China (No. 81970102) to J.S. We thank Dr. Jianwen Que, Dr. Jie Sun, Dr. Xiao Su, Dr. Xiaobo Zhou, and Dr. Chaoqun Wang for helpful discussions. We thank the Molecular and Cell Biology Core Facility, Molecular Imaging Core Facility, and Animal Core Facility at the School of Life Science and Technology, ShanghaiTech University for providing technical support.

### AUTHOR CONTRIBUTIONS

L.L. conceived the project, performed experiments, analyzed the data, and wrote the manuscript. P. Wu conceived the project and analyzed the RNA-seq and scRNA-seq data. Y.W. analyzed the RNA-seq and scRNA-seq data and performed experiments. L.M. and P. Wang performed experiments. J.S. and T.H. offered vital conceptual insights and reviewed and edited the manuscript. H.G., X.L., and X.S. provided clinical samples. L.S. offered vital conceptual insights, reviewed, and edited the manuscript. Y.X. conceived and supervised the project, analyzed the data, and wrote the manuscript.

### DECLARATION OF INTERESTS

The authors declare no competing interests.

### STAR★METHODS

Detailed methods are provided in the online version of this paper and include the following:

- [KEY RESOURCES TABLE](#)
- [EXPERIMENTAL MODEL AND STUDY PARTICIPANT DETAILS](#)
  - Animals
  - Human sample collection

- Primary cells
  - Cell line
- [METHOD DETAILS](#)
    - Fn14 antagonist treatment
    - Hydroxyproline assay
    - Histology analysis
    - Lung digestion and flow cytometry
    - AT2 organoid culture
    - Fibroblast culture
    - Bone marrow derived macrophage culture
    - Cell proliferation
    - Cell migration
    - siRNA transfection
    - Luciferase reporter gene assay
    - Western blot
    - RT-qPCR
    - Tissue preparation and immunofluorescence
    - Quantification of immunofluorescence
    - Bulk RNA-seq analysis
    - Single cell RNA-seq
  - [QUANTIFICATION AND STATISTICAL ANALYSIS](#)

### SUPPLEMENTAL INFORMATION

Supplemental information can be found online at <https://doi.org/10.1016/j.celrep.2024.115220>.

Received: April 8, 2024

Revised: November 11, 2024

Accepted: December 26, 2024

Published: January 18, 2025

### REFERENCES

1. Ley, B., Collard, H.R., and King, T.E., Jr. (2011). Clinical course and prediction of survival in idiopathic pulmonary fibrosis. *Am. J. Respir. Crit. Care Med.* 183, 431–440. <https://doi.org/10.1164/rccm.201006-0894CI>.
2. Lederer, D.J., and Martinez, F.J. (2018). Idiopathic Pulmonary Fibrosis. *N. Engl. J. Med.* 379, 797–798. <https://doi.org/10.1056/NEJMc1807508>.
3. Henderson, N.C., Rieder, F., and Wynn, T.A. (2020). Fibrosis: from mechanisms to medicines. *Nature* 587, 555–566. <https://doi.org/10.1038/s41586-020-2938-9>.
4. Martinez, F.J., Collard, H.R., Pardo, A., Raghu, G., Richeldi, L., Selman, M., Swigris, J.J., Taniguchi, H., and Wells, A.U. (2017). Idiopathic pulmonary fibrosis. *Nat. Rev. Dis. Primers* 3, 17074. <https://doi.org/10.1038/nrdp.2017.74>.
5. Moss, B.J., Ryter, S.W., and Rosas, I.O. (2022). Pathogenic Mechanisms Underlying Idiopathic Pulmonary Fibrosis. *Annu. Rev. Pathol.* 17, 515–546. <https://doi.org/10.1146/annurev-pathol-042320-030240>.
6. Shenderov, K., Collins, S.L., Powell, J.D., and Horton, M.R. (2021). Immune dysregulation as a driver of idiopathic pulmonary fibrosis. *J. Clin. Invest.* 131, e143226. <https://doi.org/10.1172/JCI143226>.
7. Buechler, M.B., Fu, W., and Turley, S.J. (2021). Fibroblast-macrophage reciprocal interactions in health, fibrosis, and cancer. *Immunity* 54, 903–915. <https://doi.org/10.1016/j.immuni.2021.04.021>.
8. Byrne, A.J., Maher, T.M., and Lloyd, C.M. (2016). Pulmonary Macrophages: A New Therapeutic Pathway in Fibrosing Lung Disease? *Trends Mol. Med.* 22, 303–316. <https://doi.org/10.1016/j.molmed.2016.02.004>.
9. Meziani, L., Mondini, M., Petit, B., Boissonnas, A., Thomas de Montpreville, V., Mercier, O., Vozenin, M.C., and Deutsch, E. (2018). CSF1R inhibition prevents radiation pulmonary fibrosis by depletion of interstitial macrophages. *Eur. Respir. J.* 51, 1702120. <https://doi.org/10.1183/13993003.02120-2017>.
10. Khalil, N., Bereznay, O., Sporn, M., and Greenberg, A.H. (1989). Macrophage production of transforming growth factor beta and fibroblast

- collagen synthesis in chronic pulmonary inflammation. *J. Exp. Med.* 170, 727–737. <https://doi.org/10.1084/jem.170.3.727>.
11. Yue, X., Shan, B., and Lasky, J.A. (2010). TGF-beta: Titan of Lung Fibrogenesis. *Curr. Enzym. Inhib.* 6. <https://doi.org/10.2174/10067>.
  12. Kim, K.K., Sheppard, D., and Chapman, H.A. (2018). TGF-beta1 Signaling and Tissue Fibrosis. *Cold Spring Harb. Perspect. Biol.* 10, a022293. <https://doi.org/10.1101/cshperspect.a022293>.
  13. Misharin, A.V., Morales-Nebreda, L., Reyfman, P.A., Cuda, C.M., Walter, J.M., McQuattie-Pimentel, A.C., Chen, C.I., Anekalla, K.R., Joshi, N., Williams, K.J.N., et al. (2017). Monocyte-derived alveolar macrophages drive lung fibrosis and persist in the lung over the life span. *J. Exp. Med.* 214, 2387–2404. <https://doi.org/10.1084/jem.20162152>.
  14. Ding, L., Liu, T., Wu, Z., Hu, B., Nakashima, T., Ullenbruch, M., Gonzalez De Los Santos, F., and Phan, S.H. (2016). Bone Marrow CD11c+ Cell-Derived Amphiregulin Promotes Pulmonary Fibrosis. *J. Immunol.* 197, 303–312. <https://doi.org/10.4049/jimmunol.1502479>.
  15. Lechner, A.J., Driver, I.H., Lee, J., Conroy, C.M., Nagle, A., Locksley, R.M., and Rock, J.R. (2017). Recruited Monocytes and Type 2 Immunity Promote Lung Regeneration following Pneumonectomy. *Cell Stem Cell* 21, 120–134.e7. <https://doi.org/10.1016/j.stem.2017.03.024>.
  16. Barkauskas, C.E., Crone, M.J., Rackley, C.R., Bowie, E.J., Keene, D.R., Stripp, B.R., Randell, S.H., Noble, P.W., and Hogan, B.L.M. (2013). Type 2 alveolar cells are stem cells in adult lung. *J. Clin. Invest.* 123, 3025–3036. <https://doi.org/10.1172/JCI68782>.
  17. Choi, J., Park, J.E., Tsagkogeorga, G., Yanagita, M., Koo, B.K., Han, N., and Lee, J.H. (2020). Inflammatory Signals Induce AT2 Cell-Derived Damage-Associated Transient Progenitors that Mediate Alveolar Regeneration. *Cell Stem Cell* 27, 366–382.e7. <https://doi.org/10.1016/j.stem.2020.06.020>.
  18. Aran, D., Looney, A.P., Liu, L., Wu, E., Fong, V., Hsu, A., Chak, S., Naikawadi, R.P., Wolters, P.J., Abate, A.R., et al. (2019). Reference-based analysis of lung single-cell sequencing reveals a transitional profibrotic macrophage. *Nat. Immunol.* 20, 163–172. <https://doi.org/10.1038/s41590-018-0276-y>.
  19. Reyfman, P.A., Walter, J.M., Joshi, N., Anekalla, K.R., McQuattie-Pimentel, A.C., Chiu, S., Fernandez, R., Akbarpour, M., Chen, C.I., Ren, Z., et al. (2019). Single-Cell Transcriptomic Analysis of Human Lung Provides Insights into the Pathobiology of Pulmonary Fibrosis. *Am. J. Respir. Crit. Care Med.* 199, 1517–1536. <https://doi.org/10.1164/rccm.201712-2410OC>.
  20. Adams, T.S., Schupp, J.C., Poli, S., Ayaub, E.A., Neumark, N., Ahangari, F., Chu, S.G., Raby, B.A., Deluliiis, G., Januszky, M., et al. (2020). Single-cell RNA-seq reveals ectopic and aberrant lung-resident cell populations in idiopathic pulmonary fibrosis. *Sci. Adv.* 6, eaba1983. <https://doi.org/10.1126/sciadv.aba1983>.
  21. Nouno, T., Okamoto, M., Ohnishi, K., Kaieda, S., Tominaga, M., Zaizen, Y., Ichiki, M., Momosaki, S., Nakamura, M., Fujimoto, K., et al. (2019). Elevation of pulmonary CD163(+) and CD204(+) macrophages is associated with the clinical course of idiopathic pulmonary fibrosis patients. *J. Thorac. Dis.* 11, 4005–4017. <https://doi.org/10.21037/jtd.2019.09.03>.
  22. Wendisch, D., Dietrich, O., Mari, T., von Stillfried, S., Ibarra, I.L., Mittermaier, M., Mache, C., Chua, R.L., Knoll, R., Timm, S., et al. (2021). SARS-CoV-2 infection triggers profibrotic macrophage responses and lung fibrosis. *Cell* 184, 6243–6261.e27. <https://doi.org/10.1016/j.cell.2021.11.033>.
  23. Chakarov, S., Lim, H.Y., Tan, L., Lim, S.Y., See, P., Lum, J., Zhang, X.M., Foo, S., Nakamizo, S., Duan, K., et al. (2019). Two distinct interstitial macrophage populations coexist across tissues in specific subtissular niches. *Science* 363, eaau0964. <https://doi.org/10.1126/science.aau0964>.
  24. Winkles, J.A. (2008). The TWEAK-Fn14 cytokine-receptor axis: discovery, biology and therapeutic targeting. *Nat. Rev. Drug Discov.* 7, 411–425. <https://doi.org/10.1038/nrd2488>.
  25. Burkly, L.C., Michaelson, J.S., Hahm, K., Jakubowski, A., and Zheng, T.S. (2007). TWEAKing tissue remodeling by a multifunctional cytokine: role of TWEAK/Fn14 pathway in health and disease. *Cytokine* 40, 1–16. <https://doi.org/10.1016/j.cyto.2007.09.007>.
  26. Burkly, L.C., Michaelson, J.S., and Zheng, T.S. (2011). TWEAK/Fn14 pathway: an immunological switch for shaping tissue responses. *Immunol. Rev.* 244, 99–114. <https://doi.org/10.1111/j.1600-065X.2011.01054.x>.
  27. Gomez, I.G., Roach, A.M., Nakagawa, N., Amatucci, A., Johnson, B.G., Dunn, K., Kelly, M.C., Karaca, G., Zheng, T.S., Szak, S., et al. (2016). TWEAK-Fn14 Signaling Activates Myofibroblasts to Drive Progression of Fibrotic Kidney Disease. *J. Am. Soc. Nephrol.* 27, 3639–3652. <https://doi.org/10.1681/ASN.2015111227>.
  28. Wilhelm, A., Shepherd, E.L., Amatucci, A., Munir, M., Reynolds, G., Humphreys, E., Reshef, Y., Adams, D.H., Hübscher, S., Burkly, L.C., et al. (2016). Interaction of TWEAK with Fn14 leads to the progression of fibrotic liver disease by directly modulating hepatic stellate cell proliferation. *J. Pathol.* 239, 109–121. <https://doi.org/10.1002/path.4707>.
  29. Culp, P.A., Choi, D., Zhang, Y., Yin, J., Seto, P., Ybarra, S.E., Su, M., Sho, M., Steinle, R., Wong, M.H.L., et al. (2010). Antibodies to TWEAK receptor inhibit human tumor growth through dual mechanisms. *Clin. Cancer Res.* 16, 497–508. <https://doi.org/10.1158/1078-0432.CCR-09-1929>.
  30. Jakubowski, A., Ambrose, C., Parr, M., Lincecum, J.M., Wang, M.Z., Zheng, T.S., Browning, B., Michaelson, J.S., Baetscher, M., Wang, B., et al. (2005). TWEAK induces liver progenitor cell proliferation. *J. Clin. Invest.* 115, 2330–2340. <https://doi.org/10.1172/JCI23486>.
  31. Girgenrath, M., Weng, S., Kostek, C.A., Browning, B., Wang, M., Brown, S.A.N., Winkles, J.A., Michaelson, J.S., Allaire, N., Schneider, P., et al. (2006). TWEAK, via its receptor Fn14, is a novel regulator of mesenchymal progenitor cells and skeletal muscle regeneration. *EMBO J.* 25, 5826–5839. <https://doi.org/10.1038/sj.emboj.7601441>.
  32. Michaelson, J.S., Cho, S., Browning, B., Zheng, T.S., Lincecum, J.M., Wang, M.Z., Hsu, Y.M., and Burkly, L.C. (2005). Tweak induces mammary epithelial branching morphogenesis. *Oncogene* 24, 2613–2624. <https://doi.org/10.1038/sj.onc.1208208>.
  33. Jin, S., Guerrero-Juarez, C.F., Zhang, L., Chang, I., Ramos, R., Kuan, C.H., Myung, P., Plikus, M.V., and Nie, Q. (2021). Inference and analysis of cell-cell communication using CellChat. *Nat. Commun.* 12, 1088. <https://doi.org/10.1038/s41467-021-21246-9>.
  34. Habermann, A.C., Gutierrez, A.J., Bui, L.T., Yahn, S.L., Winters, N.I., Calvi, C.L., Peter, L., Chung, M.I., Taylor, C.J., Jetter, C., et al. (2020). Single-cell RNA sequencing reveals profibrotic roles of distinct epithelial and mesenchymal lineages in pulmonary fibrosis. *Sci. Adv.* 6, eaba1972. <https://doi.org/10.1126/sciadv.aba1972>.
  35. Burkly, L.C. (2014). TWEAK/Fn14 axis: the current paradigm of tissue injury-inducible function in the midst of complexities. *Semin. Immunol.* 26, 229–236. <https://doi.org/10.1016/j.smim.2014.02.006>.
  36. Izicki, G., Segel, M.J., Christensen, T.G., Conner, M.W., and Breuer, R. (2002). Time course of bleomycin-induced lung fibrosis. *Int. J. Exp. Pathol.* 83, 111–119. <https://doi.org/10.1046/j.1365-2613.2002.00220.x>.
  37. Strunz, M., Simon, L.M., Ansari, M., Kathiriya, J.J., Angelidis, I., Mayr, C.H., Tsidiridis, G., Lange, M., Mattner, L.F., Yee, M., et al. (2020). Alveolar regeneration through a Krt8+ transitional stem cell state that persists in human lung fibrosis. *Nat. Commun.* 11, 3559. <https://doi.org/10.1038/s41467-020-17358-3>.
  38. Wu, H., Yu, Y., Huang, H., Hu, Y., Fu, S., Wang, Z., Shi, M., Zhao, X., Yuan, J., Li, J., et al. (2021). Progressive pulmonary fibrosis is caused by elevated mechanical tension on alveolar stem cells. *Cell* 184, 845–846. <https://doi.org/10.1016/j.cell.2021.01.020>.
  39. Sun, T., Huang, Z., Zhang, H., Posner, C., Jia, G., Ramalingam, T.R., Xu, M., Brightbill, H., Egen, J.G., Dey, A., and Arron, J.R. (2019). TAZ is required for lung alveolar epithelial cell differentiation after injury. *JCI Insight* 5, e128674. <https://doi.org/10.1172/jci.insight.128674>.

40. Jiang, P., Gil de Rubio, R., Hrycaj, S.M., Gurgczynski, S.J., Riemondy, K.A., Moore, B.B., Omary, M.B., Ridge, K.M., and Zemans, R.L. (2020). Ineffective Type 2-to-Type 1 Alveolar Epithelial Cell Differentiation in Idiopathic Pulmonary Fibrosis: Persistence of the KRT8(hi) Transitional State. *Am. J. Respir. Crit. Care Med.* 201, 1443–1447. <https://doi.org/10.1164/rccm.201909-1726LE>.
41. Kobayashi, Y., Tata, A., Konkimalla, A., Katsura, H., Lee, R.F., Ou, J., Banovich, N.E., Kropski, J.A., and Tata, P.R. (2020). Persistence of a regeneration-associated, transitional alveolar epithelial cell state in pulmonary fibrosis. *Nat. Cell Biol.* 22, 934–946. <https://doi.org/10.1038/s41556-020-0542-8>.
42. Li, Z., Wang, H., Zhu, J., Nan, N., Lin, Y., Zhuang, X., Li, L., Zhang, Y., and Huang, P. (2022). Inhibition of TWEAK/Tnfrsf12a axis protects against acute liver failure by suppressing RIPK1-dependent apoptosis. *Cell Death Discov.* 8, 328. <https://doi.org/10.1038/s41420-022-01123-0>.
43. Unudurthi, S.D., Nassal, D.M., Patel, N.J., Thomas, E., Yu, J., Pierson, C.G., Bansal, S.S., Mohler, P.J., and Hund, T.J. (2020). Fibroblast growth factor-inducible 14 mediates macrophage infiltration in heart to promote pressure overload-induced cardiac dysfunction. *Life Sci.* 247, 117440. <https://doi.org/10.1016/j.lfs.2020.117440>.
44. Deshmane, S.L., Kremlev, S., Amini, S., and Sawaya, B.E. (2009). Monocyte chemoattractant protein-1 (MCP-1): an overview. *J. Interferon Cytokine Res.* 29, 313–326. <https://doi.org/10.1089/jir.2008.0027>.
45. Rawat, K., Tewari, A., Li, X., Mara, A.B., King, W.T., Gibbons, S.L., Nnam, C.F., Kolling, F.W., Lambrecht, B.N., and Jakubzick, C.V. (2023). CCL5-producing migratory dendritic cells guide CCR5+ monocytes into the draining lymph nodes. *J. Exp. Med.* 220, e20222129. <https://doi.org/10.1084/jem.20222129>.
46. Brown, S.A.N., Ghosh, A., and Winkles, J.A. (2010). Full-length, membrane-anchored TWEAK can function as a juxtacrine signaling molecule and activate the NF- $\kappa$ B pathway. *J. Biol. Chem.* 285, 17432–17441. <https://doi.org/10.1074/jbc.M110.131979>.
47. Sanz, A.B., Sanchez-Niño, M.D., Izquierdo, M.C., Jakubowski, A., Justo, P., Blanco-Colio, L.M., Ruiz-Ortega, M., Selgas, R., Egido, J., and Ortiz, A. (2010). TWEAK activates the non-canonical NF $\kappa$ B pathway in murine renal tubular cells: modulation of CCL21. *PLoS One* 5, e8955. <https://doi.org/10.1371/journal.pone.0008955>.
48. Roos, C., Wicovsky, A., Müller, N., Salzmann, S., Rosenthal, T., Kalthoff, H., Trauzold, A., Seher, A., Henkler, F., Kneitz, C., and Wajant, H. (2010). Soluble and transmembrane TNF-like weak inducer of apoptosis differentially activate the classical and noncanonical NF- $\kappa$ B pathway. *J. Immunol.* 185, 1593–1605. <https://doi.org/10.4049/jimmunol.0903555>.
49. Hao, Y., Hao, S., Andersen-Nissen, E., Mauck, W.M., 3rd, Zheng, S., Butler, A., Lee, M.J., Wilk, A.J., Darby, C., Zager, M., et al. (2021). Integrated analysis of multimodal single-cell data. *Cell* 184, 3573–3587.e29. <https://doi.org/10.1016/j.cell.2021.04.048>.
50. Shi, T., Denney, L., An, H., Ho, L.P., and Zheng, Y. (2021). Alveolar and lung interstitial macrophages: Definitions, functions, and roles in lung fibrosis. *J. Leukoc. Biol.* 110, 107–114. <https://doi.org/10.1002/JLB.3RU0720-418R>.
51. Misharin, A.V., Morales-Nebreda, L., Mutlu, G.M., Budinger, G.R.S., and Perlman, H. (2013). Flow cytometric analysis of macrophages and dendritic cell subsets in the mouse lung. *Am. J. Respir. Cell Mol. Biol.* 49, 503–510. <https://doi.org/10.1165/rccm.2013-0086MA>.
52. Moore, B.B., Paine, R., 3rd, Christensen, P.J., Moore, T.A., Sitterding, S., Ngan, R., Wilke, C.A., Kuziel, W.A., and Toews, G.B. (2001). Protection from pulmonary fibrosis in the absence of CCR2 signaling. *J. Immunol.* 167, 4368–4377. <https://doi.org/10.4049/jimmunol.167.8.4368>.
53. Gibbons, M.A., MacKinnon, A.C., Ramachandran, P., Dhaliwal, K., Duffin, R., Phythian-Adams, A.T., van Rooijen, N., Haslett, C., Howie, S.E., Simpson, A.J., et al. (2011). Ly6Chi monocytes direct alternatively activated profibrotic macrophage regulation of lung fibrosis. *Am. J. Respir. Crit. Care Med.* 184, 569–581. <https://doi.org/10.1164/rccm.201010-1719OC>.
54. Chen, Y., Wang, W., Liu, F., Tang, L., Tang, R., and Li, W. (2015). Apoptotic effect of matrix metalloproteinases 9 in the development of diabetic retinopathy. *Int. J. Clin. Exp. Pathol.* 8, 10452–10459.
55. Cui, X., Chang, Z., Dang, T., Meng, J., Wang, P., Wu, J., and Chai, J. (2022). TNF upregulates peptidoglycan recognition protein 1 in esophageal cancer cells to clear the path to its signaling: Making the "enemy" a friend. *Arch. Biochem. Biophys.* 722, 109192. <https://doi.org/10.1016/j.abb.2022.109192>.
56. Wu, D., Wang, X., Han, Y., and Wang, Y. (2021). The effect of lipocalin-2 (LCN2) on apoptosis: a proteomics analysis study in an LCN2 deficient mouse model. *BMC Genom.* 22, 892. <https://doi.org/10.1186/s12864-021-08211-y>.
57. Heckmann, B.L., Zhang, X., Xie, X., and Liu, J. (2013). The G0/G1 switch gene 2 (G0S2): regulating metabolism and beyond. *Biochim. Biophys. Acta* 1831, 276–281. <https://doi.org/10.1016/j.bbapplied.2012.09.016>.
58. Bain, C.C., and MacDonald, A.S. (2022). The impact of the lung environment on macrophage development, activation and function: diversity in the face of adversity. *Mucosal Immunol.* 15, 223–234. <https://doi.org/10.1038/s41385-021-00480-w>.
59. Zhang, W., Wang, Y., Wan, J., Zhang, P., and Pei, F. (2019). COX6B1 relieves hypoxia/reoxygenation injury of neonatal rat cardiomyocytes by regulating mitochondrial function. *Biotechnol. Lett.* 41, 59–68. <https://doi.org/10.1007/s10529-018-2614-4>.
60. Phipps, K.D., Surette, A.P., O'Connell, P.A., and Waisman, D.M. (2011). Plasminogen receptor S100A10 is essential for the migration of tumor-promoting macrophages into tumor sites. *Cancer Res.* 71, 6676–6683. <https://doi.org/10.1158/0008-5472.CAN-11-1748>.
61. Trapnell, C., Cacchiarelli, D., Grimsby, J., Pokharel, P., Li, S., Morse, M., Lennon, N.J., Livak, K.J., Mikkelsen, T.S., and Rinn, J.L. (2014). The dynamics and regulators of cell fate decisions are revealed by pseudotemporal ordering of single cells. *Nat. Biotechnol.* 32, 381–386. <https://doi.org/10.1038/nbt.2859>.
62. Cao, J., Spielmann, M., Qiu, X., Huang, X., Ibrahim, D.M., Hill, A.J., Zhang, F., Mundlos, S., Christiansen, L., Steemers, F.J., et al. (2019). The single-cell transcriptional landscape of mammalian organogenesis. *Nature* 566, 496–502. <https://doi.org/10.1038/s41586-019-0969-x>.
63. Du, L., Lin, L., Li, Q., Liu, K., Huang, Y., Wang, X., Cao, K., Chen, X., Cao, W., Li, F., et al. (2019). IGF-2 Preprograms Maturing Macrophages to Acquire Oxidative Phosphorylation-Dependent Anti-inflammatory Properties. *Cell Metab.* 29, 1363–1375.e8. <https://doi.org/10.1016/j.cmet.2019.01.006>.
64. Zhang, S., Weinberg, S., DeBerge, M., Gainullina, A., Schipma, M., Kinchen, J.M., Ben-Sahra, I., Gius, D.R., Yvan-Charvet, L., Chandel, N.S., et al. (2019). Efferocytosis Fuels Requirements of Fatty Acid Oxidation and the Electron Transport Chain to Polarize Macrophages for Tissue Repair. *Cell Metab.* 29, 443–456.e5. <https://doi.org/10.1016/j.cmet.2018.12.004>.
65. Yu, Y.R.A., O'Koren, E.G., Hotten, D.F., Kan, M.J., Kopin, D., Nelson, E.R., Que, L., and Gunn, M.D. (2016). A Protocol for the Comprehensive Flow Cytometric Analysis of Immune Cells in Normal and Inflamed Murine Non-Lymphoid Tissues. *PLoS One* 11, e0150606. <https://doi.org/10.1371/journal.pone.0150606>.
66. Namiki, J., Suzuki, S., Shibata, S., Kubota, Y., Kaneko, N., Yoshida, K., Yamaguchi, R., Matsuzaki, Y., Masuda, T., Ishihama, Y., et al. (2022). Chitinase-like protein 3: A novel niche factor for mouse neural stem cells. *Stem Cell Rep.* 17, 2704–2717. <https://doi.org/10.1016/j.stemcr.2022.10.012>.
67. Katsura, H., Kobayashi, Y., Tata, P.R., and Hogan, B.L.M. (2019). IL-1 and TNFalpha Contribute to the Inflammatory Niche to Enhance Alveolar Regeneration. *Stem Cell Rep.* 12, 657–666. <https://doi.org/10.1016/j.stemcr.2019.02.013>.
68. Valenzi, E., Tabib, T., Papazoglou, A., Sembrat, J., Trejo Bittar, H.E., Rojas, M., and Lafyatis, R. (2021). Disparate Interferon Signaling and Shared Aberrant Basaloid Cells in Single-Cell Profiling of Idiopathic Pulmonary

- Fibrosis and Systemic Sclerosis-Associated Interstitial Lung Disease. *Front. Immunol.* 12, 595811. <https://doi.org/10.3389/fimmu.2021.595811>.
69. McCowan, J., Fercoq, F., Kirkwood, P.M., T'Jonck, W., Hegarty, L.M., Mawer, C.M., Cunningham, R., Mirchandani, A.S., Hoy, A., Humphries, D.C., et al. (2021). The transcription factor EGR2 is indispensable for tissue-specific imprinting of alveolar macrophages in health and tissue repair. *Sci. Immunol.* 6, eabj2132. <https://doi.org/10.1126/sciimmunol.abj2132>.
  70. Remmerie, A., and Scott, C.L. (2018). Macrophages and lipid metabolism. *Cell. Immunol.* 330, 27–42. <https://doi.org/10.1016/j.cellimm.2018.01.020>.
  71. Svedberg, F.R., Brown, S.L., Krauss, M.Z., Campbell, L., Sharpe, C., Clausen, M., Howell, G.J., Clark, H., Madsen, J., Evans, C.M., et al. (2019). The lung environment controls alveolar macrophage metabolism and responsiveness in type 2 inflammation. *Nat. Immunol.* 20, 571–580. <https://doi.org/10.1038/s41590-019-0352-y>.
  72. Liu, J., Liu, Y., Peng, L., Li, J., Wu, K., Xia, L., Wu, J., Wang, S., Wang, X., Liu, Q., et al. (2019). TWEAK/Fn14 Signals Mediate Burn Wound Repair. *J. Invest. Dermatol.* 139, 224–234. <https://doi.org/10.1016/j.jid.2018.05.036>.
  73. Yanaba, K., Yoshizaki, A., Muroi, E., Hara, T., Ogawa, F., Usui, A., Hasegawa, M., Fujimoto, M., Takehara, K., and Sato, S. (2009). Elevated circulating TWEAK levels in systemic sclerosis: association with lower frequency of pulmonary fibrosis. *J. Rheumatol.* 36, 1657–1662. <https://doi.org/10.3899/jrheum.081310>.
  74. Tsukui, T., Wolters, P.J., and Sheppard, D. (2024). Alveolar fibroblast lineage orchestrates lung inflammation and fibrosis. *Nature* 631, 627–634. <https://doi.org/10.1038/s41586-024-07660-1>.
  75. Chapman, H.A., Li, X., Alexander, J.P., Brumwell, A., Lorizio, W., Tan, K., Sonnenberg, A., Wei, Y., and Vu, T.H. (2011). Integrin alpha6beta4 identifies an adult distal lung epithelial population with regenerative potential in mice. *J. Clin. Invest.* 121, 2855–2862. <https://doi.org/10.1172/JCI57673>.
  76. Xi, Y., Kim, T., Brumwell, A.N., Driver, I.H., Wei, Y., Tan, V., Jackson, J.R., Xu, J., Lee, D.K., Gotts, J.E., et al. (2017). Local lung hypoxia determines epithelial fate decisions during alveolar regeneration. *Nat. Cell Biol.* 19, 904–914. <https://doi.org/10.1038/ncb3580>.
  77. Konishi, S., Tata, A., and Tata, P.R. (2022). Defined conditions for long-term expansion of murine and human alveolar epithelial stem cells in three-dimensional cultures. *STAR Protoc.* 3, 101447. <https://doi.org/10.1016/j.xpro.2022.101447>.
  78. Byles, V., Covarrubias, A.J., Ben-Sahra, I., Lamming, D.W., Sabatini, D.M., Manning, B.D., and Horng, T. (2013). The TSC-mTOR pathway regulates macrophage polarization. *Nat. Commun.* 4, 2834. <https://doi.org/10.1038/ncomms3834>.
  79. Qiu, X., Mao, Q., Tang, Y., Wang, L., Chawla, R., Pliner, H.A., and Trapnell, C. (2017). Reversed graph embedding resolves complex single-cell trajectories. *Nat. Methods* 14, 979–982. <https://doi.org/10.1038/nmeth.4402>.

## STAR★METHODS

### KEY RESOURCES TABLE

REAGENT or RESOURCE	SOURCE	IDENTIFIER
<b>Antibodies</b>		
Rabbit polyclonal anti-proSPC	Millipore	Cat#AB3786 RRID: AB_91588
Mouse monoclonal anti-ACTA2	Sigma/Aldrich	Cat#F3777 RRID: AB_476977
Rat monoclonal anti-RAGE	R&D	Cat#MAB1179 RRID: AB_2289349
Rabbit monoclonal anti-Fn14	Abcam	Cat#ab109365 RRID: AB_10864561
Rabbit polyclonal anti-phosphor-Histone H3	Merck	Cat#06570 RRID: AB_310177
Mouse monoclonal anti-β-Actin	Santa Cruz	Cat# sc-47778 RRID:AB_626632
Rabbit polyclonal anti-COL1	Abcam	Cat# ab21286 RRID: AB_446161
Rabbit monoclonal anti-SMAD2	Cell Signaling	Cat# 5339S; RRID:AB_10626777
Rabbit monoclonal anti-p-Smad2	Cell Signaling	Cat# 18338S; RRID: AB_2798798
Rabbit monoclonal anti-p65	Cell Signaling	Cat# 8242S RRID: AB_10859369
Rabbit monoclonal anti-p-p65	Cell Signaling	Cat# 3033S RRID: AB_331284
Rabbit polyclonal anti-p100/p52	Cell Signaling	Cat# 4882T RRID: AB_10695537
Mouse monoclonal anti-ARG1	Santa Cruz	Cat# sc-271430 RRID: AB_10648473
Rabbit monoclonal anti-CD11b	Santa Cruz	Cat#sc-20050 RRID: AB_626883
Rabbit monoclonal anti-ARG1	Cell Signaling	Cat#93668T RRID: AB_2800207
Goat polyclonal anti-PDGFRβ	R&D	Cat#AF1042 RRID: AB_2162633
Mouse monoclonal anti-CD104	Biolegend	Cat#123610 RRID: AB_2563544
Rat monoclonal anti-CD45	Biolegend	Cat#553080 RRID: AB_394610
Rat monoclonal anti-CD31	Biolegend	Cat#558738 RRID: AB_397097
Rat monoclonal anti-EpCAM	Biolegend	Cat#118225 RRID: AB_2563983
Mouse anti-FC blocking	Miltenyi	Cat#130-092-575 RRID: AB_2892833
Human anti-FC blocking	Miltenyi	Cat# 130-059-901 RRID: AB_2892112
Mouse monoclonal anti-CD45	BD Pharmingen	Cat#563792 RRID: AB_2869519
Rat monoclonal anti-Ly6G	BioLegend	Cat#127672 RRID: AB_2904289
Hamster monoclonal anti-CD11c	BioLegend	Cat#117314 RRID: AB_492850
Rat monoclonal anti-CD11b	BioLegend	Cat#101216 RRID: AB_312799

(Continued on next page)

**Continued**

REAGENT or RESOURCE	SOURCE	IDENTIFIER
Rat monoclonal anti-I-A/I-E	BioLegend	Cat#107621 RRID: AB_493726
Mouse monoclonal anti-CD64	BioLegend	Cat#139304 RRID: AB_10612740
Rat monoclonal anti-CD24	BioLegend	Cat#101826 RRID: AB_2563508
Rat monoclonal anti-Siglec F	Thermo Fisher	Cat#53-1702-82 RRID: AB_2784747
Mouse monoclonal anti-HTII-280	Terrace Biotech	Cat#TB-27AHT2 RRID: AB_2832931
Goat polyclonal anti-IgM-AF488	Thermo Fisher	Cat#A-21042 RRID: AB_2535711
Mouse monoclonal anti-EpCAM	Biolegend	Cat#324206 RRID: AB_756080
Rat monoclonal anti-CD31	Biolegend	Cat#303122 RRID: AB_2562149
<b>Chemicals, peptides, and recombinant proteins</b>		
Tamoxifen	Sigma/Aldrich	T5648-5G
Bleomycin	Sinopharm Chemical Reagent	XW90419341
L524-0366	TargetMol	T8570
TWEAK	MedChemExpress	HY-P7309
TGF $\beta$ 1	R&D	240-B-010
SB431542	Selleck	S1067
Fibronectin	Merck/Millipore	FC010
Fetal bovine serum	Ausbian	VS500T
BASIC RPMI 1640	Thermo/Life/Invitrogen	C11875500CP
Advance D-MEM/F-12	Thermo/Life/Invitrogen	12634010
DMEM	Thermo/Life/Invitrogen	31053036
CHIL3	MedChemExpress	HY-P7845
IL18	R&D	9139-IL-010/CF
Matrigel™	Corning	356231
penicillin/streptomycin	Thermo	15140122
Glutamax	Thermo	35050061
Amphotericin B	Sigma	E3789
DNase I	Roche	10104159001
Collagenase type I	Thermo Fisher	17100017
Dispase II	Invitrogen	17105041
Red Blood Cell Lysis Buffer	Beyotime	C3702
<b>Critical commercial assays</b>		
Hydroxyproline Assay	Sigma/Aldrich	MAK008
Click EdU Alexa 647 imaging	Thermo/Life/Invitrogen	C10340
CellTiter-Glo® Luminescent Cell Viability Assay	Promega	G7571
Hematoxylin and Eosin Staining Kit	Yeasen	60524ES60
BeyoClick™ EdU Cell Proliferation Kit with Alexa Fluor 488	Byotitime	C0071S
Dual-Luciferase® Reporter Assay System	Promega	E1910
EastepTM Super Total RNA Extraction Kit	Promega	LS1040
Direct-zol™ RNA MicroPrep	Zymo Research	R2061
HiScript III RT SuperMix for qPCR	Vazyme	R323-01
ChamQ Universal SYBR qPCR Master Mix	Vazyme	Q711-03
Pierce BCA protein assay	Thermo/Life/Invitrogen	23227

(Continued on next page)

**Continued**

REAGENT or RESOURCE	SOURCE	IDENTIFIER
<b>Deposited data</b>		
Raw sequencing files for fibroblast RNA-seq	This paper	GEO: GSE262923
Raw sequencing files for immune cell scRNA-seq	This paper	GEO: GSE262928
The publicly available human lung scRNA-seq data	Habermann et al. <sup>34</sup>	GEO: GSE135893
The publicly available mouse lung scRNA-seq data	Strunz et al. <sup>37</sup>	GEO: GSE141259
The publicly available mouse lung scRNA-seq data	Tsukui et al. <sup>74</sup>	GEO: GSE210341
The publicly available mouse lung scRNA-seq data	Aran et al. <sup>18</sup>	GEO: GSE111664
<b>Experimental models: Cell lines</b>		
Human: HEK293T	ATCC	Cat# SNL-015
<b>Experimental models: Organisms/strains</b>		
Mouse: <i>Fn14</i> -KO mice	This paper	N/A
Mouse: <i>Cx3cr1-CreERT2</i> mice	Shanghai Model Organisms Center	NM-KI-200157
Mouse: C57BL/6J	Shanghai Jihui Laboratory Animal Care Co. Ltd.	N/A
Mouse: <i>R26-LSL-tdTomato</i> mice	Harold Chapman Lab (UCSF)	N/A
<b>Oligonucleotides</b>		
siRNA targeting sequence: Ccl2: #1 GAUCAGAACCUACAACUUU, #2 GUGAAGUUGACCGGUAAA, #3 CCGUAAAUCUGAAGCUAAU.	This paper	N/A
siRNA targeting sequence: Ccl5: #1 CUUGCAGUCGUGUUUGUCA, #2 CAAGAAUACAUCAACUAUU.	This paper	N/A
siRNA targeting sequence: Rela: #1 GUGUGGACAAGAAGCGAAATT, #2 UUUCGCUUUCUUGGUCCACACTT.	This paper	N/A
siRNA targeting sequence: Relb: #1 GGACCUAUGAGACCUUCAATT, #2 UUGAAGGUCUCAUAGGUCCCTT.	This paper	N/A
Primers for RT-qPCR, see Table S4	N/A	N/A
<b>Recombinant DNA</b>		
Plasmid: 4X Smad-binding element (SBE)	Addgene, Cambridge, MA	N/A
Plasmid: Renilla luciferase	Promega, Madison, WI	N/A
<b>Software and algorithms</b>		
ImageJ	NIH	<a href="https://www.proteinatlas.org/">https://www.proteinatlas.org/</a>
Graphpad Prism 9	Graphpad	<a href="https://www.graphpad.com/scientificsoftware/prism/">https://www.graphpad.com/scientificsoftware/prism/</a>
R v4.2.2	CRAN project	<a href="https://www.r-project.org/">https://www.r-project.org/</a>
FlowJo	BD Biosciences	<a href="https://www.flowjo.com/">https://www.flowjo.com/</a>

## EXPERIMENTAL MODEL AND STUDY PARTICIPANT DETAILS

### Animals

All animals were housed and treated according to the procedures approved by the Animal Ethics Committee of ShanghaiTech University and all animal experiments were done in compliance with ethical guidelines and the approved protocols. CRISPR/Cas9 technology was used to generate *Fn14*-KO mice by targeting exon 1 of *Fn14* gene in C57BL/6J background. After zygote microinjection and embryo transplantation, genomic DNA from tail tip of F0 mice were sequenced and positive founders were selected for mating with wild-type C57BL/6J mice. Genomic DNA from F1 pups was sequenced to confirm germline transmission of edited chromosome and absence of off-target hits. *Cx3cr1-CreERT2*<sup>18</sup> and *R26-LSL-tdTomato* mice<sup>75</sup> were previously described. For lineage tracing, 200 mg/kg tamoxifen (Sigma) dissolved in corn oil were intraperitoneally injected into *Cx3cr1-CreERT2*; *R26-LSL-tdTomato* mice every other day starting from the day of bleomycin injury and sacrificed on day 3 and day 7 for flow cytometry.

For bleomycin injury model, WT C57BL/6J mice and *Fn14*-KO mice (8–14-week-old) of both sexes were used in equal proportions. The animals were randomized on the basis of body weights to minimize variation between the two groups. The mice were intratracheally instilled with 50 µL sterile saline or bleomycin (1.7 mg/kg body weight, Nippon Kayaku), weighed twice a week and sacrificed at indicated days for follow-up experiments.

For EdU incorporation experiments, the mice were intraperitoneally injected with 100 mg 5'-Ethynyl-2'-deoxyuridine (EdU) (Thermo, C10340) in PBS on day 1, 3, 5, 7 after bleomycin or saline instillation (day 0) and were sacrificed on day 8. FACS and immunofluorescence were performed according to the manufacturer's protocol for Click-iT EdU Alexa Fluor 647 imaging kit (Thermo, C10340).

#### Human sample collection

All human normal and fibrotic tissue samples were obtained from Huadong Hospital Affiliated to Fudan University or Tongji University Affiliated Shanghai Pulmonary Hospital approved by the Human Ethics Committee of Huadong Hospital or Shanghai Pulmonary Hospital, respectively. Participants provided written informed consent. Lung tissues were collected from donor lungs declined for transplantation and IPF patients undergoing lung transplantation classified as Non-identifiable Otherwise Discarded Human Tissues. Information on human donors is listed in [Table S3](#).

#### Primary cells

Primary cells, including alveolar epithelial cells, lung fibroblasts and macrophages were isolated as described in the methods details section below. Human sample information is listed in [Table S3](#). Mice were age (8–14 weeks) and gender (male or female) matched.

#### Cell line

The human embryonic kidney 293 (HEK293T) cell line were sourced from ATCC and cultured under standard conditions (5% CO<sub>2</sub> and 37°C) in DMEM supplemented with 10% fetal bovine serum (Ausbian, VS500T), 1% penicillin/streptomycin (Thermo, 15140122) and 1% Glutamax (Thermo, 35050061). Tested free of mycoplasma contamination.

#### METHOD DETAILS

##### **Fn14 antagonist treatment**

L524-0366 (TargetMol, T8570) were dissolved in 5% DMSO + 30% PEG400 + 5% Tween-80 + 60% ddH<sub>2</sub>O as previously described.<sup>42,43</sup> Nine mg/kg L524-0366 was injected daily starting from the day after bleomycin by intraperitoneal injection until the mice were sacrificed on day 14. The same volume of the dissolving buffer was injected as a vehicle control.

##### **Hydroxyproline assay**

The left lungs were snap frozen and used for hydroxyproline assay. Snap-frozen mouse lungs were ground into tissue powder, hydrolyzed in 1 mL of 6 M hydrochloric acid at 120°C for 3 h in a pressure-tight polypropylene vial with PTFE-lined cap (Sigma-Aldrich, TMO362800-0020). Then the sample was mixed and centrifuged at 10,000g for 10 min. Five µL of the supernatant was transferred to a 96-well plate and dried in a 60°C oven. The manufacturer's protocol for the hydroxyproline kit (Sigma-Aldrich, MAK008) was followed with slight modifications for subsequent steps. Briefly, 100 µL of Chloramine T/Oxidation Buffer Mixture was added in each reaction well and incubated at room temperature for 5 min. Then 100 µL of the Diluted DMAB Reagent was added to each well and incubated for 60 min at 60°C. Finally, the absorbance was measured at 560 nm.

##### **Histology analysis**

The small intestines, kidneys and hearts were fixed with 4% paraformaldehyde (PFA, Sigma, 16005) for 24 h at 4°C and the pancreas, livers and lungs were fixed for 1 h at room temperature before embedded in OCT (Sakura, 4583). Subsequently, 4 mm cryosections were cut and stained with hematoxylin and eosin (H&E) (Yeasen, 60524ES60).

##### **Lung digestion and flow cytometry**

Human distal lung tissue was processed as previously described.<sup>76</sup> Human distal lung tissue was washed twice in sterile PBS and once in Hank's Buffered Saline Solution (HBSS) (Invitrogen, 14175079), then compressed to remove liquid and dissected into small pieces. 15 U/mL Dispase II (Invitrogen, 17105041), 225 U/mL Collagenase type I (Thermo Fisher, 17100017), 0.2 mg/mL DNase I (Roche, 10104159001) and 1% penicillin/streptomycin (Thermo, 15140122) in HBSS was used to digest the tissue for 1 h at 37°C. Then the tissue was dissociated by gentleMACS Dissociator (Miltenyi) and incubated in the digestion buffer for another 1 h. 250 ng/mL Amphotericin B (Sigma, E3789) was added during the final 30 min of the digestion. The cell suspension was sequentially filtered through 100 µm, 70 µm, and 40 µm strainers. Red blood cells were removed using Red Blood Cell Lysis Buffer (Beyotime, C3702). After Fc blocking (1:20; Miltenyi, 130-059-901), the cells were stained with anti-HTII-280 (1:80; Terrace Biotech, TB-27AHT2), anti-human IgM-AF488 (1:500, Thermo Fisher, A-21042) BV395 anti-human/mouse CD45 (1:1000; Biolegend, 563792), PE anti-human EpCAM (1:400; Biolegend, 324206), BV605 anti-human CD31 (1:100; Biolegend, 303122), eFluor 780 (1:2000; Invitrogen, 65-0865-14) and sorted. Human lung fibroblasts were sorted as live/CD45<sup>+</sup>/CD31<sup>+</sup>/EpCAM<sup>+</sup> cells.

Mouse lung cells were isolated as previously described.<sup>76,77</sup> Mouse lungs were perfused with 1 mL of Dispase II, digested for 45 min at room temperature and subsequently mashed. Then DNase I (1:150) digestion at 37°C for 15 min. The cell suspension was sequentially filtered through 100 µm, 70 µm, and 40 µm strainers. Red blood cells were removed using Red Blood Cell Lysis Buffer, the cells were stained with PE anti-mouse CD104 (1:150; Biolegend, 123610), FITC anti-mouse CD45 (1:1000; Biolegend, 553080), FITC anti-mouse CD31 (1:750; Biolegend, 558738), BV421 anti-mouse EpCAM (1:500; Biolegend, 118225) and eFluor 780 (1:2000; Invitrogen, 65-0865-14) after anti-mouse Fc blocking (1:20; Miltenyi, 130-092-575). Mouse AT2 cells were sorted as live/CD45<sup>-</sup>/CD31<sup>-</sup>/EpCAM<sup>+</sup>/CD104<sup>-</sup>, lung fibroblasts cells were sorted as live/CD45<sup>-</sup>/CD31<sup>-</sup>/EpCAM<sup>-</sup>, and immune cells were sorted as live/CD45<sup>+</sup>/CD31<sup>-</sup>/EpCAM<sup>-</sup>. For FACS analysis of mouse lung macrophages, single cell preparations were stained with BUV395 anti-mouse CD45 (1:1000; BD Pharmingen, 563792), PE-Cy5 anti-mouse Ly-6G (1:1000; BioLegend, 127672), AF647 anti-mouse CD11c (1:1000; BioLegend, 117314), PE-Cy7 anti-mouse CD11b (1:200; BioLegend, 101216), AF700 anti-mouse I-A/I-E (1:1000; BioLegend, 107621), PE anti-mouse CD64 (1:100; BioLegend, 139304), BV421 anti-mouse CD24 (1:100; BioLegend, 101826), AF488 anti-mouse Siglec F (1:100; Thermo, 53-1702-82), BV605 anti-mouse CD64 (1:100; BioLegend, 139323).

### AT2 organoid culture

Flow-sorted primary lung AT2 cells and macrophages were plated and cultured in 3D organoids as previously described.<sup>77</sup> 500 mouse AT2 cells and 5000 macrophages resuspended in AT2 Maintenance Medium (AMM) were mixed 1:1 with Matrigel (Corning, 356231) and a 40 µL droplet was placed in the center of a well in a 24-well plate. Matrigel was allowed to solidify for 30 min at 37°C and followed by addition of 500 µL of AMM. Medium was changed every 3 days. The organoids were harvested for fixation and immunofluorescence on day 10. For CHIL3 (MedChemExpress, HY-P7845) and IL18 (R&D, 9139-IL-010/CF) treatment, 1000 mouse AT2 cells were resuspended in AMM and treated with 200 ng/mL CHIL3 or IL18 on day 2, followed by harvesting on day 10.

### Fibroblast culture

Primary mouse lung fibroblasts (MLF), human lung fibroblasts (HLF) and IPF HLF were isolated from single cell suspension of fresh lung tissue by flow sorting of CD45<sup>-</sup> EpCAM<sup>-</sup> CD31<sup>-</sup> cells, and cultured in DMEM (Invitrogen, 31053036) supplemented with 10% fetal bovine serum (Ausbrian, VS500T), 1% penicillin/streptomycin (Thermo, 15140122) and 1% Glutamax (Thermo, 35050061) at 37°C, 5% CO<sub>2</sub> atmosphere. For human lung fibroblast culture, 250 ng/mL Amphotericin B (Sigma, E3789) was added in the medium to prevent fungal infections. For the treatment, primary human or mouse lung fibroblasts were seeded at the density of 40,000–50,000 cells/well in 12-well plates and treated with recombinant human TWEAK (MedChemExpress, HY-P7309) at 10, 30, 100 ng/mL, 4 ng/mL TGFβ1 (R&D, 240-B-010), 10 µM SB431542 (Selleck, S1067) or 25 µM L524-0366 (TargetMol, T8570). For cytokine screening, mouse lung fibroblasts were treated with LPS (100 ng/mL), IL6 (20 ng/mL), IL13 (20 ng/mL), TNFα (100 ng/mL), TGFβ1 (4 ng/mL), IL10 (20 ng/mL), Wnt3a (100 ng/mL), PDGFBB (100 ng/mL), IL4 (20 ng/mL), IL1β (20 ng/mL) or 10% FBS. Mouse lung fibroblasts were stimulated for 48 h and human lung fibroblasts were stimulated for 72 h.

To collect conditioned medium (CM), the fibroblasts were treated with or without recombinant human TWEAK at the concentration of 30 ng/mL for 5 days. The cell culture supernatant was collected, centrifuged at 3000 rpm for 10 min to remove cell debris and concentrated 20x with Amicon Ultra-0.5 Centrifugal Filter Unit (Merck/Millipore, UFC5003BK).

### Bone marrow derived macrophage culture

Bone marrow derived macrophage (BMDM) culture and polarization were performed as previously described.<sup>78</sup> BMDM culture were performed as followings: mouse femur and tibia were ground, resuspended with BASIC RPMI 1640 (Invitrogen, C11875500CP) and filtered. Six million cells were cultured in BASIC RPMI 1640 supplemented with 10% fetal bovine serum (Ausbrian, VS500T), 1% penicillin/streptomycin, 25% L929 supernatant, 100X HEPES (Invitrogen, 15630080) in 10-cm non-treated tissue culture dish.

### Cell proliferation

Primary fibroblasts were seeded at the density of 15,000 cells/well in 96-well plates and treated with recombinant human TWEAK at 10, 30, 100 ng/mL or 10% fetal bovine serum in serum-free DMEM medium for 48 h followed by CellTiter-Glo Luminescent assay (Promega, G7571) or BeyoClick EdU-488 labeling and imaging (Beyotime, C0071S).

### Cell migration

Transparent Polyester (PET) membrane inserts (Falcon, 353097, 8.0 µm pore size) for 24 well format was used for fibroblast and macrophage transwell assay. For fibroblasts migration, fibroblasts were seeded on top of the inserts at the density of 20,000 cells/well in serum-free DMEM medium and allowed to settle for 30 min before TWEAK was added to the bottom plate at the concentration of 30 ng/mL in serum-free DMEM medium. 10% fetal bovine serum was used as positive control. The fibroblasts were cultured for 16 h before harvesting.

For macrophage migration, the upper membrane of inserts was coated with 20 ng/mL Fibronectin (Merck, FC010) overnight. On the next day, macrophages were seeded at the density of 40,000 cells/well in 100 µL serum-free RPMI medium. Conditioned medium from fibroblasts treated with or without TWEAK were add to the lower chamber and the macrophages were cultured for 16 h before harvesting.

Non-migrating cells on top of the inserts were removed by swabbing. The cells on the bottom were fixed with 4% paraformaldehyde (PFA, Sigma, 16005) for 15 min, stained with 1% crystal violet (Solarbio, G1062-500) for 20 min and imaged Zeiss Axio Zoom V16 (ZEISS). The cells on the entire bottom membrane were counted.

### siRNA transfection

Fibroblasts were seeded at the density of 200,000 cells/well in a 6-well plate and transfected with 30 nM indicated siRNAs (GenePharma) using RNAiMAX (Invitrogen, 13778150). Transfected cells were cultured without perturbation for 24 h prior to TWEAK stimulation and then harvested after 48 h for gene expression analysis or 72 h for conditioned medium collection. The siRNA target sequences are listed in the [key resources table](#).

### Luciferase reporter gene assay

4X Smad-binding element (SBE) plasmid (Addgene, Cambridge, MA) was co-transfected in HEK293T (ATCC, SNL-015) cells with Renilla luciferase plasmid (Promega, Madison, WI) using Lipofectamine 2000 (Invitrogen, 11668019) according to the manufacturer's protocol. Twenty-four hours post transfection, 4 ng/mL TGF $\beta$ 1 alone or together with 30 ng/mL TWEAK was added to each well in serum-free DMEM medium. Six hours later, luciferase activity assay was performed according to the manufacturer's protocol for the Dual-luciferase reporter assay system (Promega, E1910).

### Western blot

Snap-frozen mouse lungs were ground into tissue powder and lysed in RIPA buffer (50mM Tris-HCl, pH 7.5, 150mM NaCl, 1% deoxycholate, 0.1% SDS, 1% Triton X-100) supplemented with Protease Inhibitor Cocktail (Roche, 11697498001), Phosphatase Inhibitor Cocktail (Millipore, 524625) and 1 mM phenylmethyl sulfonyl fluoride. The lysates were quantified using Pierce BCA kit (Thermo, 23227). Equal amounts of protein lysates were separated by SDS-PAGE, transferred to Immobilon-P PVDF Membrane (Merck, IPVH00010) and blotted for: Fn14 (1:300; Abcam, ab109365),  $\beta$ -Actin (1:1000; Santa Cruz, sc-47778), pro-SPC (1:3000; Millipore, AB3786), COL1 (1:250; Abcam, ab21286), SMAD2 (1:500; Cell Signaling, 5339S), p-SMAD2 (1:500; Cell Signaling, 18338S), p-p65 (1:500; Cell Signaling, 3033S), p65 (1:500; Cell Signaling, 8242S), p100/p52 (1:500; Cell Signaling, 4882T).

### RT-qPCR

Snap-frozen lungs were ground into tissue powder and total RNA was purified using EastepTM Super Total RNA extraction kit (Promega, LS1040) with genomic DNA removed with DNase I. RNA Extraction Kit (Zymo Research, R2061) was used to isolate RNA from freshly sorted cells or cultured cells. Complementary DNA was synthesized using HiScript III RT SuperMix for qPCR (Vazyme, R323-01). Quantitative PCR reactions were performed in technical triplicates using ChamQ SYBR qPCR Mix (Vazyme, Q711-03). Relative standard curve method was used for quantification and the expression levels were calculated by normalization to *Hprt*. The primer sequences are listed in [Table S4](#).

### Tissue preparation and immunofluorescence

Freshly dissected mouse lungs were processed and stained as previously described.<sup>76</sup> The lungs were inflated with 4% PFA and 50% OCT (SAKURA, 4583) dissolved in PBS for 1 h, then incubated with 30% sucrose and 50% OCT overnight followed by embedding in OCT. 6 mm cryosections were cut, fixed with 4% PFA for additional 5 min, incubated with 0.1% sodium borohydride (Sigma, 213462) and then blocked and stained in PBS plus 1% bovine serum albumin (Sigma, A1933), 5% horse serum (ATCC, 30-2040), 0.1% Triton X-100 (Sinopharm, 30188928). Paraffin embedded human specimens were deparaffinized followed by antigen retrieval using Tris-EDTA (Gibco, 25300054) before blocking and staining as stated above. The following antibodies were used: rabbit anti-proSPC (1:3000; Millipore, AB3786), FITC-conjugated mouse anti-ACTA2(1:200; Sigma, F3777), rat anti-ECAD (1:100; Invitrogen, 131900), rat anti-RAGE (1:400; R&D, MAB1179), rabbit anti-Fn14 (1:300; Abcam, ab109365), rabbit anti-phospho-Histone H3 (1:500; Merck, 06-570), mouse anti-ARG1 (1:100; Santa Cruz, sc-271430), mouse anti-CD11b (1:100; Santa Cruz, sc-20050), rabbit anti-ARG1 (1:100; Cell Signaling, 93668T), goat anti-PDGFR $\beta$  (1:50; R&D, AF1042).

### Quantification of immunofluorescence

To quantify ACTA2 $^+$  myofibroblast and SFTPC $^+$  AT2 areas, the whole lobes were imaged with Nikon Ti2-E CSU-W1 Sora Camera (Nikon, Japan). The ACTA2 $^+$  areas of the entire lobe were quantified using ImageJ with a plugin for machine learning-based image segmentation and smooth muscle cell staining around airways and blood vesicles was excluded. SFTPC $^+$  areas were manually outlined and measured by ImageJ.

### Bulk RNA-seq analysis

Primary mouse lung fibroblasts were seeded at the density of 50,000 cells/well in 12-well plates and treated with or without 10, 30, 100 ng/mL recombinant human TWEAK protein (MedChemExpress, HY-P7309) for 48 h, with two biological replicates per condition. Total RNA was extracted and sequenced by Illumina HiSeq sequencing platform. The raw paired end reads were trimmed and quality controlled by Skewer with default parameters. For each sample, STAR software was used to compare the preprocessed sequences with the reference genome sequences of sequenced species. For all samples, StringTie was used to count the original sequence of

known genes, and FPKM was used to calculate the expression of known genes. According to the experimental design, DESeq2 was used to screen differentially expressed genes between different groups, and differentially expressed genes satisfying the range of  $| \log_2FC | \geq 1$  and  $p$  value  $\leq 0.05$  were screened between the two groups. In addition, functional-enrichment analysis including GO and KEGG were performed to identify with clusterProfiler package.

### Single cell RNA-seq

CD45<sup>+</sup> cells from 4 mice each group (WT saline, WT bleomycin, Fn14 KO Saline, Fn14 KO Bleomycin) were sorted by FACS and captured by Chromium (10X Genomics, Pleasanton, CA). Libraries were sequenced using the Illumina NovaSeq 6000. Sequencing was targeted to 52437 cells in the CD45<sup>+</sup> library with sequencing depth of 43611 reads/cell. Cell Ranger v6.1.1 was used to conduct quality control on the raw data. The “Seurat” R package was used to perform single-cell RNA-seq analyses. Count matrices were merged using Seurat version 4.3.0,<sup>49</sup> and a percentage of mitochondrial genes were calculated. Cells containing less than 200 identified genes or more than 25% of reads arising from mitochondrial genes were removed. After quality control, 53921 cells were further analyzed for their gene expression profiles. For normalization and feature selection, the Seurat functions “NormalizeData”, “FindVariableFeatures” (n.features = 3000) and “ScaleData” were used. Two-dimensional representations were generated using the top 10 PCA vectors as input to the “RunUMAP” functions. Cells were clustered using the “FindClusters” function (resolutions = 0.8). Each cell was classified according to its expression of canonical cell markers. For further grouping definition of macrophages, we extracted macrophage subsets by “subset” function, and then re-normalized and clustered them according to the above method. The selected PC and resolution are respectively 10 and 0.8.

To define the Inflammatory score and Oxidative phosphorylation score, we downloaded the gene sets termed “HALLMARK\_OXIDATIVE\_PHOSPHORYLATION”.<sup>77</sup> These scores were then evaluated by using Seurat (“AddModuleScore” function) with default parameters.

To predict the differentiation trajectories of different types of macrophages, we initiated the pseudotime trajectory in the macrophage’s population, using a custom function described in the Monocle 3 documentation to automatically select the starting point for the pseudotime analysis.<sup>79</sup> To compare the Monocle and Seurat clustering results, the number of cells and frequency of cluster membership overlap between Monocle and Seurat was calculated.

The published scRNA-seq database of IPF lung (GSE135893)<sup>34</sup> and mouse bleomycin database (GSE111664, GSE141259, GSE210341)<sup>18,37,74</sup> was reanalyzed using R package Seurat V4.3.0. Cell communication analysis was performed by using R package CellChat V1.6.0<sup>33</sup> with default parameters.

### QUANTIFICATION AND STATISTICAL ANALYSIS

Custom scripts in R v4.2.2 were utilized for RNA-seq and scRNA-seq data analysis and plotting. All other statistical calculations were performed using GraphPad Prism. Variance for all group data is expressed as mean  $\pm$  s.e.m. Statistical details of experiments can be found in corresponding figure legends, including the statistical tests used, exact value and definition of n. Differences were considered to be statistically significant when  $p$  value  $<0.05$ . Sample sizes were determined based on previous experience with similar experiments.